

# Diplomarbeit

## Performance Evaluation of Differential Modulation in LTE-Downlink

ausgeführt zum Zwecke der Erlangung des akademischen Grades  
eines Diplom-Ingenieurs

unter der Leitung von  
Univ.Prof. Dipl.-Ing. Dr.techn. Markus Rupp  
Dipl.-Ing. Michal Šimko  
Dipl.-Ing. Stefan Schwarz

Institute of Telecommunications

eingereicht an der Technischen Universität Wien  
Fakultät für Elektrotechnik und Informationstechnik

von  
Markus Hofer  
Matrikelnr.: 0626418  
Bernhard 23  
3323 Neustadt  
Wien, Jänner 2013

---

I hereby certify that the work presented in this thesis is my own,  
and the work of other authors is properly cited.

*Markus Hofer*

Markus Hofer  
Neustadtl, January 2013

---

# Abstract

This diploma thesis evaluates the performance of differential modulation applied to the 3GPP Long Term Evolution downlink. The focus specifically lies on single input single output transmissions with only one user.

The Long Term Evolution downlink is based on channel estimation. The reference symbols, required for channel estimation cannot be used to transmit data, which reduces the spectral efficiency. In order to increase the spectral efficiency, in this thesis noncoherent detection is considered. With noncoherent detection no channel knowledge is needed. Thus, the reference symbols for channel estimation are no longer required. Two basic modulation schemes, namely the frequency first and the time first modulation scheme, are presented. Their performance is investigated both for frequency selective linear time-invariant and linear time-variant channels and compared to coherent detection with least squares channel estimation and zero forcing equalization. As performance criteria the bit error ratio and the throughput over the signal to noise ratio are considered. In the investigations it is discovered that coherent detection outperforms conventional noncoherent detection. To improve the efficiency also multiple symbol differential detection is applied. Furthermore, the correct selection of the modulation scheme for different channels is discussed.

---

# Kurzfassung

Diese Diplomarbeit evaluiert die Effizienz differentieller Modulation angewendet auf den 3GPP Long Term Evolution downlink. Die Arbeit konzentriert sich dabei auf Systeme mit einer Sendeantenne und einer Empfangsantenne für Übertragungen mit nur einem Nutzer.

Der Long Term Evolution downlink basiert auf Kanalschätzung. Für Kanalschätzung werden Referenzsymbole benötigt die nicht zur Datenübertragung benutzt werden können. Dies reduziert die spektrale Effizienz. Um die spektrale Effizienz zu erhöhen wird in dieser Diplomarbeit nicht kohärente Detektion betrachtet. Bei nicht kohärenter Detektion ist die Kanalinformation nicht erforderlich. Daher werden die Referenzsymbole für die Kanalschätzung nicht benötigt. Es werden zwei Modulationsschemata mit dem Namen frequency first modulation und time first modulation vorgestellt. Diese werden auf ihre Leistungsfähigkeit in frequenzselektiven linearen zeit-invarianten und linearen zeit-varianten Kanälen untersucht und mit kohärenter Detektion mit least squares Kanalschätzung und zero forcing Entzerrung verglichen. Als Effizienzkriterien werden die Bitfehlerrate und der Durchsatz herangezogen. In den Untersuchungen wird festgestellt, dass die Leistung von kohärenter Detektion höher als die Leistung der konventionellen nicht kohärenten Detektion ist. Um die Effizienz zu steigern wird differentielle Detektion mit mehreren Symbolen angewendet. Zusätzlich wird die korrekte Wahl des Modulationsschemas für verschiedene Kanäle behandelt.

---

# Contents

<b>1</b>	<b>Introduction</b>	<b>1</b>
<b>2</b>	<b>Overview of Differential Modulation in LTE</b>	<b>3</b>
2.1	General Description of Differential Modulation . . . . .	3
2.2	Overview of LTE . . . . .	8
2.3	Application of Differential Modulation in LTE . . . . .	9
2.4	System Model . . . . .	11
2.5	Simulation Setup . . . . .	15
<b>3</b>	<b>Block Fading</b>	<b>17</b>
3.1	Frequency selective and frequency non selective channels . . . . .	18
3.1.1	Selection of the modulation scheme . . . . .	19
3.1.2	Uncoded BER and throughput for different channels . . . . .	20
3.1.3	Coded throughput in an ITU PedB channel . . . . .	24
3.2	Multiple Symbol Differential Detection . . . . .	26
3.3	Multiple Symbol Differential Sphere Decoding . . . . .	30
3.3.1	Uncoded BER and throughput with multiple symbol dif- ferential sphere decoding (MSDSD) . . . . .	35
3.3.2	Coded throughput with MSDSD . . . . .	39
<b>4</b>	<b>Fast Fading</b>	<b>43</b>
4.1	Selection of the Differential Modulation scheme . . . . .	43
4.1.1	Frequency first versus time first modulation scheme in an ITU VehA channel . . . . .	44
4.1.2	Modulation scheme for AWGN channels, Rayleigh flat fading channels and channels with equal correlation . . . . .	45
4.1.3	Estimation of the speed at which to switch between the frequency first and the time first modulation scheme . . . . .	45
4.2	Multiple Symbol Differential Sphere Decoding in Fast Fading Channels . . . . .	47
4.2.1	Uncoded BER of 4-DPSK in an ITU VehA channel . . . . .	48

4.2.2 Coded throughput in an ITU VehA channel . . . . .	49
<b>5 Conclusion</b>	<b>51</b>
<b>A Acronyms</b>	<b>53</b>
<b>Bibliography</b>	<b>55</b>

---

## List of Figures

2.1	General transmission system . . . . .	3
2.2	Example for a 64-APSK constellation . . . . .	6
2.3	Signal structure of LTE in the time domain . . . . .	9
2.4	Time-frequency grid visualizing the frequency first differential modulation scheme for one resource block-pair . . . . .	10
2.5	OFDM transmit signal processing chain with differential modulation . . . . .	12
2.6	OFDM receive signal processing chain with differential modulation	12
3.1	BER of the frequency first modulation scheme compared to the time first modulation scheme with 64-DAPSK in an ITU PedB channel . . . . .	19
3.2	Uncoded throughput of the frequency first modulation scheme compared to the time first modulation scheme with 64-DAPSK in an ITU PedB channel . . . . .	20
3.3	BER of noncoherent detection compared to coherent detection in an AWGN channel . . . . .	21
3.4	Throughput of noncoherent detection compared to coherent detection in an AWGN channel . . . . .	21
3.5	BER of noncoherent detection compared to coherent detection in an ITU PedB channel . . . . .	22
3.6	Throughput of noncoherent detection compared to coherent detection in an ITU PedB channel . . . . .	23
3.7	Throughput of 4-DPSK in different channels . . . . .	23
3.8	Coded throughput in PedB . . . . .	25
3.9	Multiple symbol detection in frequency direction . . . . .	26
3.10	BER of 4-DPSK with MSDSD in an AWGN channel . . . . .	35
3.11	Uncoded Throughput of 4-DPSK with MSDSD in an AWGN channel . . . . .	36
3.12	BLER of 4-DPSK with MSDSD in an AWGN channel . . . . .	36
3.13	BER of 4-DPSK with MSDSD in an ITU PedB channel . . . . .	38

---

3.14	Uncoded Throughput of 4-DPSK with MSDSD in ITU PedB . . .	38
3.15	Coded Throughput of MSDSD in an AWGN channel . . . . .	39
3.16	4-DPSK and 4-QAM for $R = 0.853$ and $R = 0.926$ . . . . .	40
3.17	Coded Throughput of MSDSD in an ITU PedB channel . . . . .	42
4.1	Coded throughput of the time first modulation versus the frequency first modulation in an ITU VehA channel . . . . .	44
4.2	BER of frequency first versus time first modulation scheme in a fast fading ITU VehA channel with SNR = 30 dB . . . . .	47
4.3	Uncoded BER performance of noncoherent detection in an ITU VehA channel with $v = 100$ km/h . . . . .	49
4.4	Coded throughput of MSDSD in an ITU VehA channel for $v = 100$ km/h . . . . .	50

## List of Tables

2.1	Amplitude information bit mapping for different DAPSK types . . .	6
2.2	General simulation setup . . . . .	16
3.1	CQI with corresponding modulation and coding scheme . . . . .	25



# 1 Introduction

According to recent studies in [1, 2], the global demand on mobile data traffic more than doubles every year. The cause of this exponential growth in data rate are mobile devices, especially smartphones, netbooks and tablets. Additionally new communication technologies like machine-to-machine communication lead to an increase of mobile data traffic.

To cope with this demand it is necessary to improve the spectral efficiency of current mobile communication standards such as 3GPP Universal Mobile Telecommunications System (UMTS) Long Term Evolution (LTE) [3]. LTE systems require channel estimation for coherent detection. Channel estimation can get computationally demanding, especially for rapidly varying channels. Furthermore, the reference symbols (RS) required for channel estimation cannot be used to transmit data, which decreases the spectral efficiency. A way to increase the spectral efficiency is to reduce the RS overhead for channel estimation. Therefore, in this thesis noncoherent detection is considered. Noncoherent detection offers the possibility to receive data without knowledge of the channel, thus the RS for channel estimation are not required. Although this can provide a higher peak spectral efficiency, the disadvantage of noncoherent detection is a performance loss compared to coherent detection in terms of signal-to-noise ratio (SNR). In [4, 5], differential modulation was investigated for different transmission techniques. The performance of differential modulation in LTE, however, has not yet been evaluated.

This diploma thesis investigates the performance of differential modulation in a single input single output (SISO) Orthogonal Frequency Division Multiplex-

ing (OFDM) system with parameters chosen such that it is equivalent to the LTE downlink. The focus lies on the single user case.

The layout of this thesis is as follows: Chapter 2 presents an overview of differential modulation in LTE and shows two basic modulation schemes that can be applied to the LTE downlink. Chapter 3 discusses the performance of differential modulation for a block fading environment and Chapter 4 investigates the performance in a fast fading environment. Finally, Chapter 5 concludes the presented work and gives an outlook on possible future research areas.

The following notation is used throughout this thesis:  $E\{x\}$  denotes the expected value of a random variable  $x$ ,  $\text{diag}\{\mathbf{x}\}$  represents a diagonal matrix with components of the vector  $\mathbf{x}$  on its main diagonal and  $(\cdot)^T$  and  $(\cdot)^H$  denote the transpose and the conjugate transpose of a matrix, respectively. Furthermore,  $\det(\cdot)$  is the determinant of a square matrix and  $\exp(\cdot)$  is the natural exponential function. For the presented simulation results the confidence intervals are calculated for 95%.

## 2 Overview of Differential Modulation in LTE

This chapter comprises an overview of differential modulation in LTE. To that extent, Section 2.1 presents a general description of differential modulation. Section 2.2 describes the basic characteristics of LTE. Section 2.3 shows how to apply differential modulation to the LTE downlink and Section 2.4 presents the system model that is used in this thesis. Finally, Section 2.5 presents the simulation setup.

### 2.1 General Description of Differential Modulation

For a general description of differential modulation, Figure 2.1 depicts a transmission system consisting of the differential modulator, the channel and non-coherent detection. In the following description each of these parts is explained separately.

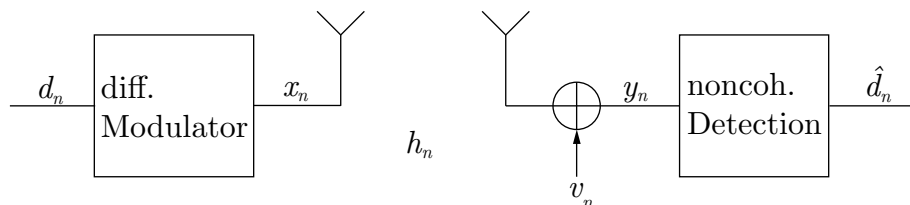


Figure 2.1: General transmission system

The first component shown in Figure 2.1 is the differential modulator. In differential modulation the information symbol  $d_n$  is encoded in the transition between two consecutive data symbols  $x_n$  and  $x_{n-1}$ , i.e.,

$$x_n = x_{n-1}d_n \quad \text{with} \quad \{x_n, x_{n-1}\} \in \mathcal{X}, d_n \in \mathcal{D} \quad \text{and} \quad n \geq 2. \quad (2.1)$$

Here,  $\mathcal{X}$  and  $\mathcal{D}$  are the symbol alphabets of the data and information symbols, respectively. For the symbol alphabet  $\mathcal{X}$  in most cases  $M$ -Phase Shift Keying (PSK) [6] or  $M$ -Amplitude and Phase Shift Keying (APSK) [7, 8] are utilized. Here,  $M$  denotes the size of the symbol alphabet. The data symbol  $x_1$  is called reference symbol and can be chosen freely from the symbol alphabet  $\mathcal{X}$ . It is the initial value of the transmission and is used as a starting point of the differential modulation process. The transmitter and receiver are both informed about the chosen reference symbol  $x_1$ . Each information symbol  $d_n$  represents a vector  $\mathbf{b}^n = [b_1^n, \dots, b_p^n]$  of  $p = \log_2(M)$  information bits. It describes the transition between the previous and the current data symbol and is element of the symbol alphabet  $\mathcal{D}$ . The information is either transmitted by a phase change or by an amplitude and phase change between  $x_n$  and  $x_{n-1}$ . This is referred to as Differential Phase Shift Keying (DPSK) and Differential Amplitude and Phase Shift Keying (DAPSK), respectively.

In DPSK, the  $p$  information bits are mapped to one of the symbols in the  $M$ -PSK symbol alphabet  $\mathcal{D} = \{e^{j\Delta\varphi i_P} | i_P = 0, \dots, 2^p - 1\}$  of  $M$  equally distributed phase states using Gray mapping. The phase difference between two consecutive states is  $\Delta\varphi = 2\pi/M = 2\pi/2^p$ . As an example for DPSK, consider binary Differential PSK (BDPSK), with  $p = 1$  and  $\Delta\varphi = 180^\circ$ . Hence, for instance, the information bit 1 is transmitted by a phaseshift of  $180^\circ$  ( $d_n = -1$ ) between  $x_n$  and  $x_{n-1}$ , whereas the information bit 0 is transmitted by a phaseshift of  $0^\circ$  ( $d_n = 1$ ). Because of the periodicity of the phase, the symbol alphabet  $\mathcal{X}$  is the same as  $\mathcal{D}$ .

In order to increase the spectral efficiency, in DAPSK the information is transmitted both by an amplitude change (Differential Amplitude Shift Keying (DASK)) and a phase change (DPSK). The  $M$ -APSK symbol alphabet consists of  $M$  constellation points that are arranged in  $2^q$  concentric amplitude rings (Amplitude Shift Keying (ASK)) with  $2^{(p-q)}$  equally distributed phase states (PSK). Each APSK information symbol represents  $p$  information bits and can be written as

$$d_n = \gamma_n\beta_n \quad \text{with} \quad \gamma_n \in \mathcal{R}, \beta_n \in \mathcal{V} \quad \text{and} \quad \mathcal{D} = \mathcal{R} \cup \mathcal{V}. \quad (2.2)$$

Here,  $\gamma_n$  is the amplitude information symbol that is taken from the  $2^q$ -ASK symbol alphabet  $\mathcal{R}$  and  $\beta_n$  is the phase information symbol that is taken from the  $2^{(p-q)}$ -PSK symbol alphabet  $\mathcal{V}$ . The information bit vector  $\mathbf{b}^n$  is divided into the amplitude information bit vector  $\mathbf{b}_\gamma^n = [b_{\gamma,1}^n, \dots, b_{\gamma,q}^n]$  of size  $q$  and into the phase information bit vector  $\mathbf{b}_\beta^n = [b_{\beta,1}^n, \dots, b_{\beta,p-q}^n]$  of size  $p - q$ , i.e.,  $\mathbf{b}^n = [\mathbf{b}_\gamma^n, \mathbf{b}_\beta^n]$ . In order to obtain  $\gamma_n$ , the amplitude information bits  $\mathbf{b}_\gamma^n$  are mapped to one of the concentric amplitude rings taken from the ASK symbol alphabet  $\mathcal{R} = \{\alpha^{i_A} | i_A = 0, \dots, 2^q - 1\}$ . Here,  $\alpha > 1$  is the amplitude ratio between two consecutive amplitude rings. A possible bit mapping can be found in Table 2.1. To obtain the symbol  $\beta_n$  the phase information bits  $\mathbf{b}_\beta^n$  are mapped to one of the PSK symbols in the symbol alphabet  $\mathcal{V} = \{e^{j\Delta\varphi i_P} | i_P = 0, \dots, 2^{(p-q)} - 1\}$  with  $\Delta\varphi = 2\pi/2^{(p-q)}$ . Thus, to generate the DAPSK data symbol

$$x_n = a_n s_n \quad \text{with} \quad a_n \in \mathcal{A}, s_n \in \mathcal{S} \quad \text{and} \quad \mathcal{X} = \mathcal{A} \cup \mathcal{S}, \quad (2.3)$$

and considering the standard differential modulation process of Equation (2.1),  $x_n$  writes as [9]

$$\begin{aligned} x_n &= d_n x_{n-1} \\ &= \gamma_n \beta_n \cdot a_{n-1} s_{n-1} \\ &= \alpha^{(i_A(\gamma_n) + i_A(a_{n-1})) \bmod 2^q} \cdot e^{j\Delta\varphi(i_P(\beta_n) + i_P(s_{n-1}))}. \end{aligned} \quad (2.4)$$

Here,  $i_A(\cdot)$  and  $i_P(\cdot)$  are the indices of the radius and the phase arguments, respectively. With the help of the  $2^q$  modulo operation in Equation (2.4) it is ensured that the symbol  $a_n$  is taken from the same ASK symbol alphabet as  $\gamma_n$ , i.e.,  $\mathcal{A} = \mathcal{R}$ . Furthermore, since the phase is periodic also  $\mathcal{S} = \mathcal{V}$ . Thus for DAPSK again  $\mathcal{X}$  is the same as  $\mathcal{D}$ .

An example for the symbol alphabet of 64-APSK is presented in Figure 2.2. It consists of 4 concentric amplitude rings ( $q = 2$ ) and 16 phase states with a phase difference of  $\Delta\varphi = 360^\circ/16 = 22.5^\circ$  between two consecutive states. Note that in this example the symbol alphabet is normalized such that the average transmit symbol energy is 1. The most common 16-APSK symbol alphabet consists of 2 concentric amplitude rings ( $q = 1$ ) and 8 phase states with a phase difference of  $\Delta\varphi = 360^\circ/8 = 45^\circ$  between each state.

After differential modulation, the data symbols are transmitted over the channel to the receiver (see Figure 2.1). In order to illustrate the basic idea behind the detection process of differential modulation, the channel is assumed to be

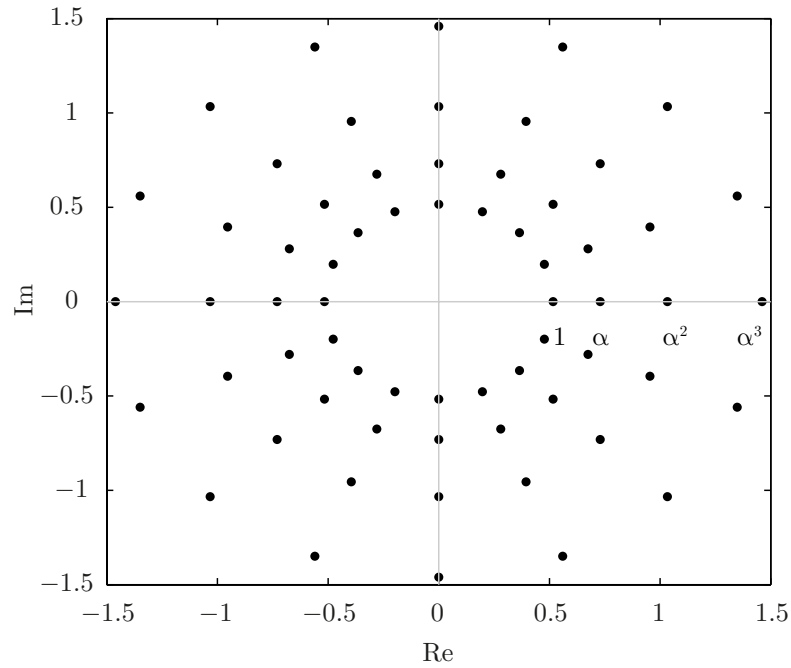


Figure 2.2: Example for a 64-APSK constellation

16-DAPSK ( $q = 1$ )				64-DAPSK ( $q = 2$ )					
$a_n$		$b_{\gamma,1}^n$		$a_n$		$b_{\gamma,1}^n, b_{\gamma,2}^n$			
		0	1			00	01	11	01
		$\gamma_n$				$\gamma_n$			
		1	$\alpha$			1	$\alpha$	$\alpha^2$	$\alpha^3$
$a_{n-1}$	1	1	$\alpha$	$a_{n-1}$	1	1	$\alpha$	$\alpha^2$	$\alpha^3$
	$\alpha$	$\alpha$	1		$\alpha$	$\alpha$	$\alpha^2$	$\alpha^3$	1
	1	1	$\alpha$		$\alpha^2$	$\alpha^2$	$\alpha^3$	1	$\alpha$
	$\alpha$	$\alpha$	1		$\alpha^3$	$\alpha^3$	1	$\alpha$	$\alpha^2$

Table 2.1: Amplitude information bit mapping for different DAPSK types

constant over frequency. The received data symbol  $y_n$  at time index  $n$  can then be written as

$$y_n = h_n x_n + v_n, \quad (2.5)$$

where  $h_n$  and  $v_n$  represent the channel coefficient and the noise at time index  $n$ , respectively.

At the receiver, in the simplest noncoherent detection scheme, the received

symbol  $y_n$  at time index  $n$  is divided by the symbol  $y_{n-1}$  of the previous time index  $n - 1$ , resulting in

$$\tilde{d}_n = \frac{y_n}{y_{n-1}}. \quad (2.6)$$

A quantizer  $\mathcal{Q}$  converts  $\tilde{d}_n$ , which due to the noise could be any complex-valued number, to a valid information symbol  $\hat{d}_n$  that is taken from the symbol alphabet  $\mathcal{D}$ ,

$$\hat{d}_n = \mathcal{Q} \left\{ \tilde{d}_n \right\} = \mathcal{Q} \left\{ \frac{y_n}{y_{n-1}} \right\}. \quad (2.7)$$

For  $\mathcal{Q}$  a minimum distance quantizer is assumed, i.e., the detected symbol  $\hat{d}_n$  is chosen as the valid symbol  $d \in \mathcal{D}$ , which is closest to  $\tilde{d}_n$ . In BDPSK, e.g., if the phase lies between  $90^\circ$  and  $270^\circ$   $\tilde{d}_n$  is quantized to  $\hat{d}_n = -1$  and otherwise it is quantized to  $\hat{d}_n = 1$ .

Finally,  $\hat{d}_n$  is demapped to the estimated bit vector  $\hat{\mathbf{b}}^n = [\hat{b}_1^n, \dots, \hat{b}_p^n]$  of length  $p$  according to the symbol alphabet  $\mathcal{D}$ . In DPSK Gray mapping is applied for the demapping process.

In DAPSK the quantization of amplitude and phase is performed separately. In this case  $\tilde{d}_n$  is calculated as

$$\tilde{d}_n = \frac{y_n}{y_{n-1}} = \tilde{\gamma}_n \tilde{\beta}_n, \quad (2.8)$$

where  $\tilde{\gamma}_n$  corresponds to the transmitted amplitude information and  $\tilde{\beta}_n$  to the transmitted phase information. The quantizer converts  $\tilde{\gamma}_n$  and  $\tilde{\beta}_n$  to the detected amplitude information symbol  $\hat{\gamma}_n$  and the detected phase information symbol  $\hat{\beta}_n$ , respectively,

$$\hat{d}_n = \mathcal{Q} \left\{ \tilde{\gamma}_n \tilde{\beta}_n \right\} = \hat{\gamma}_n \hat{\beta}_n. \quad (2.9)$$

For the quantization of  $\tilde{\beta}_n$  the symbol alphabet  $\mathcal{V}$  is utilized. In the amplitude quantization process,  $\tilde{\gamma}_n$  is assigned to one of the  $2^{q+1} - 1$  possible amplitude ratios of  $\hat{\gamma}_n$ . As decision thresholds the geometric means of two adjacent amplitude ratios are used, i.e.,

$$\begin{aligned}\hat{\gamma}_{i_{th}} &= \sqrt{\alpha^{i_{th}} \cdot \alpha^{i_{th}+1}} \\ &= \alpha^{i_{th}} \cdot \sqrt{\alpha} \quad \text{with } i_{th} \in \{-2^q + 1, \dots, 2^q - 1\}.\end{aligned}\quad (2.10)$$

After the quantization, the phase of  $\hat{\beta}_n$  is demapped according to the phase regions of the symbol alphabet  $\mathcal{V}$ . From that process the estimated phase information bit vector  $\hat{\mathbf{b}}_\beta^n = [\hat{b}_{\beta,1}^n, \dots, \hat{b}_{\beta,p-q}^n]$  of length  $p - q$  is obtained. In the amplitude demapping process  $\hat{\gamma}_n$  is demapped to the estimated amplitude information bit vector  $\hat{\mathbf{b}}_\gamma^n = [\hat{b}_{\gamma,1}^n, \dots, \hat{b}_{\gamma,q}^n]$ . A bit mapping for the corresponding decision regions of 64-DAPSK is shown in [7, Figure 4].

## 2.2 Overview of LTE

The transmission in LTE downlink is based on OFDM. OFDM systems convert a broadband frequency selective wireless channel into  $K$  orthogonal narrow-band frequency flat channels (subcarriers) by means of a Fast Fourier Transform (FFT) and application of a cyclic prefix (CP) [10]. The variable  $K$  represents the FFT size. The OFDM subcarrier spacing in LTE can be either 7.5 kHz or 15 kHz, where 7.5 kHz is used for multicast/broadcast transmissions. Furthermore, LTE supports multiple input multiple output (MIMO) and adaptive modulation and coding to adjust the transmission rate to the varying channel characteristics. The channel quality indicator (CQI) is utilized to indicate the preferred modulation and coding scheme for the current channel conditions.

The structure of the LTE signal in the time domain is shown in Figure 2.3. An LTE transmission consists of frames with a length of 10 ms, which are divided into ten equally sized subframes of length  $T_{\text{frame}} = 1$  ms. Each of these subframes has two slots of the same length  $T_{\text{slot}} = 0.5$  ms. A slot consists of a number of OFDM symbols including the CP. Depending on the size of the cyclic prefix (extended or normal), each slot consists of either six or seven OFDM symbols.

The smallest physical resource in LTE is called resource element (RE) and represents one subcarrier during one OFDM symbol. The REs are grouped to resource blocks. Each resource block (RB) consists of 12 consecutive subcarriers in the frequency domain and one 0.5 ms slot in the time domain. In the case of normal CP length, a RB thus consists of  $12 \times 7 = 84$  REs. Two of



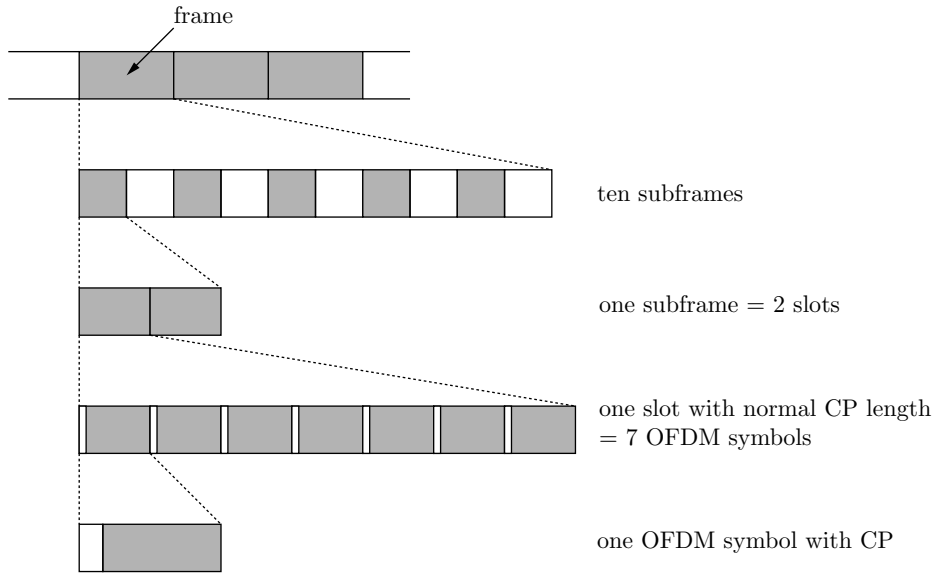


Figure 2.3: Signal structure of LTE in the time domain

these resource blocks are grouped to a resource block-pair (RBP). The number of available RBPs varies between 6 and 100, corresponding to a transmission bandwidth of 1.4 MHz to 20 MHz.

### 2.3 Application of Differential Modulation in LTE

In order to evaluate the performance of differential modulation in LTE, consider an OFDM system with parameters chosen such that it is equivalent to the LTE downlink (see Section 2.5). The smallest scheduling unit in the LTE downlink is a RBP. Figure 2.4 shows the RBP in the concept of a time-frequency grid. The vertical axis represents the frequency direction (i.e., subcarriers), the horizontal axis the time direction (i.e., OFDM symbols). As mentioned above, a RB with normal CP length consists of 84 REs, which are represented as squares in the grid. Thus a RBP consist of  $2 \times 84 = 168$  REs. Each RE contains a modulated symbol. In the following explanation a resource element of a RBP of the  $n$ -th OFDM symbol and the  $k$ -th subcarrier is indexed as  $x_{n,k}$  with  $n \in \{1, 2, \dots, 14\}$  and  $k \in \{1, 2, \dots, 12\}$ .

For the differential modulation process two scenarios are considered:

- Frequency first modulation

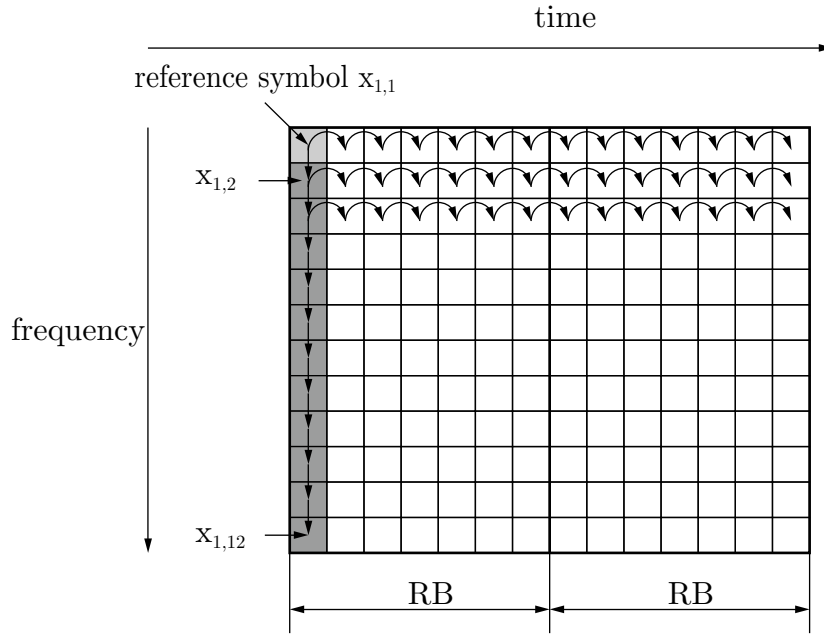


Figure 2.4: Time-frequency grid visualizing the frequency first differential modulation scheme for one resource block-pair

- Time first modulation

Both modulation schemes use the resource element  $x_{1,1}$  as a reference symbol, marked light grey in the left upper corner of Figure 2.4. It does not convey information and it is utilized as initial value of the data transmission. In the frequency first modulation scheme the differential modulation starts with modulating in the frequency direction,

$$x_{n,k} = x_{n,k-1}d_{n,k} \text{ with } k \in \{2, 3, \dots, 12\} \text{ and } n = 1. \quad (2.11)$$

For instance, the data symbol  $x_{1,2}$  is obtained by multiplying the data symbol  $x_{1,1}$  with the information symbol  $d_{1,2}$ . The modulation in the frequency direction results in the data symbols  $x_{1,1}$  to  $x_{1,12}$  on the twelve consecutive subcarriers. Subsequently, these symbols are taken as reference symbols for modulation in the time direction according to the same principle as before,

$$x_{n,k} = x_{n-1,k}d_{n,k} \text{ with } n \in \{2, 3, \dots, 14\} \text{ and } k \in \{1, 2, \dots, 12\}. \quad (2.12)$$

The modulation in the time direction is performed over the whole RBP, each subcarrier at a time. Figure 2.4 illustrates the modulation process. The first column of the grid represents the data symbols of the first OFDM symbol.

Each of these data symbols serves as a reference symbol for differential modulation in the time direction. E.g., the symbol  $x_{1,1}$  serves as a reference symbol for modulation in the time direction on the first subcarrier,  $x_{1,2}$  is taken as a reference symbol for modulation in the time direction on the second subcarrier and so on.

The time first modulation scheme works similar to the frequency first modulation scheme, except that the modulation starts in the time direction and the obtained symbols are taken as reference symbols for modulation in the frequency direction. With these modulation schemes only the symbol  $x_{1,1}$  does not convey any information.

For coherent detection, LTE defines 8 reference symbols for channel estimation in a SISO transmission [10]. These symbols cannot be utilized to transmit information, therefore, differential modulation potentially provides a higher maximum throughput. Exactly speaking, in the noncoherent case, employing the proposed differential modulation scheme, 167 REs can be used to transmit information. In the coherent case only 160 REs are available. Thus noncoherent transmission offers a

$$\frac{167 - 160}{160} = 4.37\% \quad (2.13)$$

higher possible peak throughput in SISO.

## 2.4 System Model

The system model used throughout this thesis to describe the OFDM system with differential modulation is depicted in Figures 2.5 and 2.6. The first part of the signal processing chain represents the channel encoder that encodes a block of  $L_u$  information bits  $u$  with a coding rate  $R$ . This results in the coded information bits  $c$  of length  $L_c$ . Coding inserts redundant information bits, which enables the receiver to correct a certain amount of bit errors [11]. The lower the coding rate, the higher is the amount of errors that can be corrected. The coding rate is defined as  $R = L_u/L_c$ . For the channel encoder, turbo coding [12] with rate matching (see [10, Section 10.1.1.4]) is applied. After coding,  $c$  is divided into coded information bit vectors  $\mathbf{b}^{n,k}$  of length  $p$ . These vectors are mapped to the information symbols  $d_{n,k}$  according to the corresponding symbol alphabet, i.e., either  $M$ -PSK or  $M$ -APSK. Subsequently, differential modulation is performed as explained in the previous

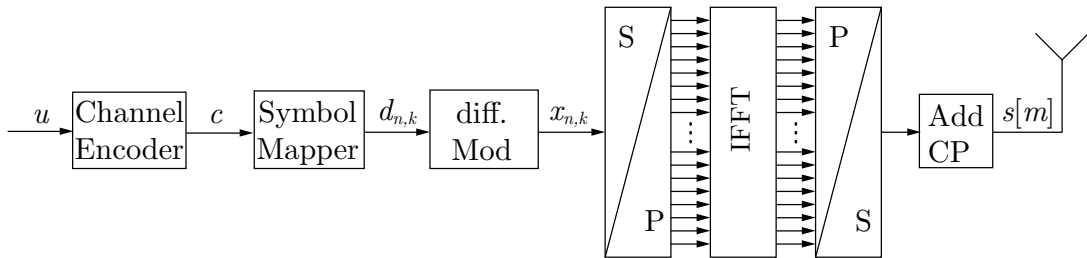


Figure 2.5: OFDM transmit signal processing chain with differential modulation

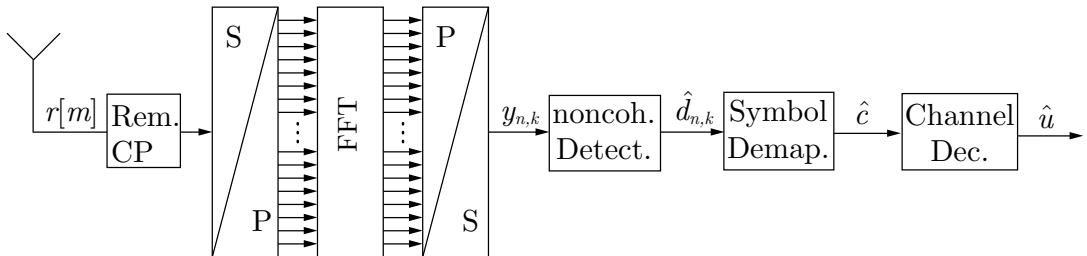


Figure 2.6: OFDM receive signal processing chain with differential modulation

section. This is followed by a serial-to-parallel conversion and an Inverse Fast Fourier Transform (IFFT) that converts the signal into the time domain. Then a parallel-to-serial conversion is performed and the CP is appended. The CP is assumed to be long enough so that no inter symbol interference (ISI) from the previous OFDM symbol occurs. The digital-to-analog converter in connection with an up-converter, which are not shown in Figure 2.5, generate the signal that is transmitted over the channel to the receiver.

For a finite impulse response (FIR) linear time-variant (LTV) channel that fulfills the wide-sense stationary uncorrelated scattering (WSSUS) [11] assumptions, the received signal  $r[m]$  in complex baseband [11] at the discrete time instant  $m$  can be written as

$$\begin{aligned}
 r[m] &= h[m, l] * s[m] + w[m] \\
 &= \sum_{l=0}^{L-1} h[m, l] s[m - l] + w[m],
 \end{aligned} \tag{2.14}$$

with

$$s[m] = \sum_{n=-\infty}^{\infty} s_n[m - nJ], \quad (2.15)$$

and

$$s_n[m] = \sqrt{K} \sum_{k=0}^{K-1} x_{n,k} e^{j2\pi \frac{kn}{K}} = \text{IFFT}_{k \rightarrow m} \{x_{n,k}\}, \quad k < K \quad (2.16)$$

The discrete-time channel impulse response  $h[m, l]$  of length  $L$  is obtained by sampling the continuous channel impulse response  $h(t, \tau)$  [11] with a sampling frequency  $F_s = K \cdot F$ . Here,  $K$  denotes the FFT size and  $F$  denotes the subcarrier spacing. For the simulations in this thesis the continuous channel impulse response is generated based on the tapped-delay line model given in [13]. The transmitted signal  $s[m]$  is the summation of  $s_n[m]$ , which is the IFFT of the  $n$ -th OFDM symbol (see Equation (2.16)). The variable  $J$  in the definition of  $s[m]$  denotes the discrete time duration of one OFDM symbol and  $w[m]$  is a sample of an AWGN process.

The receiver (Figure 2.6) is assumed to be perfectly synchronized to the transmitter in time and frequency. The received radio frequency signal is down-converted and sampled, producing the received signal  $r[m]$ . After removal of the CP the base band signal is transformed to the frequency domain, resulting in the received data symbol  $y_{n,k}$  of the  $n$ -th OFDM symbol and the  $k$ -th subcarrier. For an LTV channel with negligible inter carrier interference (ICI),  $y_{n,k}$  can be written as

$$y_{n,k} = H_{n,k} x_{n,k} + v_{n,k}. \quad (2.17)$$

Here,  $H_{n,k}$  denotes the channel at subcarrier  $k$  during the  $n$ -th OFDM symbol. It can be calculated as the FFT of  $h[m, l]$ . The noise  $v_{n,k}$  is assumed to be independent zero mean complex Gaussian with variance  $\sigma_v^2$ . The received data symbols  $y_{n,k}$  are subsequently used to detect the transmitted information symbols  $d_{n,k}$ .

Employing the basic detection scheme of Section 2.1, the information symbols are detected similarly to Equation (2.7). In the frequency first modulation scheme the detection begins in the frequency direction by estimating the in-

formation symbols of the first OFDM symbol, i.e.,

$$\hat{d}_{n,k} = \mathcal{Q} \left\{ \frac{y_{n,k}}{y_{n,k-1}} \right\} \quad \text{with } n = 1 \quad \text{and } k \in \{2, \dots, 12\}. \quad (2.18)$$

This is followed by estimating the remaining information symbols on each subcarrier in the time direction

$$\hat{d}_{n,k} = \mathcal{Q} \left\{ \frac{y_{n,k}}{y_{n-1,k}} \right\} \quad \text{with } n \in \{2, \dots, 12\} \quad \text{and } k \in \{1, \dots, 12\}. \quad (2.19)$$

The detection process in the time first modulation scheme is similar to that of the frequency first modulation scheme, except that the detection begins in the time direction on the first subcarrier. This is followed by estimating the remaining information symbols of each OFDM symbol in the frequency direction. If the channel  $H_{n,k}$  varies between two received symbols, errors can be introduced by the quantizer  $\mathcal{Q}$ , irrespective of the noise. As an example consider the detection process in the frequency direction. The symbol  $\tilde{d}_{n,k}$  can be written as

$$\begin{aligned} \tilde{d}_{n,k} &= \frac{y_{n,k}}{y_{n,k-1}} \\ &= \frac{H_{n,k}x_{n,k} + v_{n,k}}{H_{n,k-1}x_{n,k-1} + v_{n,k-1}}. \end{aligned} \quad (2.20)$$

Neglecting the impact of the noise, this can be rewritten as

$$\begin{aligned} \tilde{d}_{n,k} &\approx \frac{H_{n,k}x_{n,k}}{H_{n,k-1}x_{n,k-1}} \\ &= \underbrace{\frac{|H_{n,k}|}{|H_{n,k-1}|}}_{\text{amplitude error}} \cdot \underbrace{\frac{e^{\phi_{H_{n,k}}}}{e^{\phi_{H_{n,k-1}}}}}_{\text{phase error}} \cdot \frac{x_{n,k}}{x_{n,k-1}}. \end{aligned} \quad (2.21)$$

If  $H_{n,k}$  is different from  $H_{n,k-1}$  an additional amplitude and phase error is in-

roduced to  $\tilde{d}_{n,k}$ . This can lead to a wrongly quantized  $\hat{d}_{n,k}$ , i.e.,  $\hat{d}_{n,k} \neq d_{n,k}$ , irrespective of the noise. Consider, e.g., the case when APSK is used as modulation alphabet. If the channel introduces an amplitude error that is greater than half of the geometric mean of two adjacent amplitude ratios (see Equation (2.10)), or a phase error that is greater than  $\Delta\varphi/2$ , the quantization process  $\mathcal{Q}$  leads to an error. These errors can cause a residual bit error floor that decreases the overall performance of the system.

After noncoherent detection, the detected information symbols  $\hat{d}_{n,k}$  are demapped to the estimated coded information bit vectors  $\hat{\mathbf{b}}^{n,k}$  of length  $p$ . These vectors are concatenated to the estimated coded information bit stream  $\hat{c}$ , which is decoded to the estimated information bit stream  $\hat{u}$ .

## 2.5 Simulation Setup

To evaluate the performance of differential modulation the system model presented in Section 2.4 is implemented in Matlab. A system bandwidth of 1.4 MHz (6 RBPs) and a subcarrier spacing of 15 kHz is assumed. The carrier frequency is set to 2.5 GHz. The symbol alphabets tested for differential modulation are 4-PSK, 16-APSK and 64-APSK. Numerical results in [14] showed that the best bit error ratio (BER) performance over general fading channels is achieved with an amplitude ring ratio  $\alpha = 2$  for 16-APSK and  $\alpha = 1.4$  for 64-APSK. It is assumed that the receiver perfectly knows the amplitude ratio  $\alpha$ . For the simulations the average symbol energy of the transmitted data symbols is normalized to 1. The coding rates  $R$  of the different CQI levels are implemented according to [15]. In the simulations we consider a single user scenario, i.e, the codeword of the user spans all RBPs of the subframe. The simulation results are compared to coherent detection using Quadrature Amplitude Modulation (QAM) with least squares (LS) channel estimation and zero forcing (ZF) equalizer. In SISO LTE, 8 symbols are defined for channel estimation. The channel coefficients between the channel estimation positions are obtained by linear interpolation [16]. The simulation parameters are summarized in Table 2.2.

The performance of the system is determined by the BER and the throughput over SNR. The throughput is referred to as the number of information bits  $L_u$  inside a correctly received subframe. This means in the uncoded case ( $R = 1$ ), if there is only one bit error in the whole subframe all information is regarded as

Parameter	Abbreviation	Value
Bandwidth	$B$	1.4 MHz
FFT size	$K$	128
Subcarrier spacing	$F$	15 kHz
Sampling frequency	$F_s$	1.92 MHz
Number of data subcarriers	$N_{sub}$	72
Carrier frequency	$f_c$	2.5 GHz
$\alpha_{16}$ APSK		2
$\alpha_{64}$ APSK		1.4
Channel estimation		LS
Equalization		ZF

---

Table 2.2: General simulation setup

false and discarded. In the coded scenario ( $R < 1$ ) the bit errors are evaluated after decoding. If there is only one error in the decoded information bit stream, the subframe is regarded as false and discarded.



## 3 Block Fading

This chapter discusses the performance of differential modulation in the SISO LTE downlink in the case of block fading. Block fading channels can be classified into frequency selective and frequency non selective channels. Section 3.1 gives a mathematical description for this classification. The simulation results indicate that noncoherent detection leads to a performance loss compared to coherent detection. Section 3.2 discusses means to decrease this performance loss by multiple symbol differential detection. This, however, leads to an increased complexity in the detection process. Section 3.3 shows how to reduce the complexity with the help of the sphere decoding algorithm.

In block fading the coherence time of the channel is assumed to be long enough so that the channel impulse response stays approximately constant over one subframe. According to [17] the coherence time of the channel is defined as

$$T_c = \frac{1}{4D_s}, \quad (3.1)$$

where  $D_s$  is the Doppler spread. The Doppler spread is the largest difference between the Doppler shifts of different multi-path components and can be written as

$$D_s = \max_{i,j} |f_{D_i} - f_{D_j}|, \quad (3.2)$$

with  $f_{D_i}$  being the Doppler shift of the  $i$ -th path of the channel impulse

response. The Doppler shift is calculated as

$$f_D = f_c \frac{v}{c_0}. \quad (3.3)$$

Here,  $f_c$  is the carrier frequency of the system,  $v$  is the relative velocity between transmitter and receiver and  $c_0$  is the speed of light.

For LTE, the subframe duration length is 1 ms, which means for block fading  $T_c > 1\text{ms}$  is required. Thus

$$D_s < \frac{1}{4T_c} \quad (3.4)$$

$$D_s < 250 \text{ Hz}. \quad (3.5)$$

Assuming the Clarke's model [17], where  $D_s = 2f_D$ , the maximum relative velocity for block fading calculates as

$$v < \frac{f_D c_0}{f_c} \quad (3.6)$$

$$v < 15 \text{ m/s} \quad (3.7)$$

For the following simulations a linear time-invariant (LTI) channel over one subframe is assumed, thus block fading is guaranteed to be fulfilled.

### 3.1 Frequency selective and frequency non selective channels

A measure for the frequency selectivity of the channel is the coherence bandwidth. According to [17] it is defined as

$$W_c = \frac{1}{2T_d}, \quad (3.8)$$

where  $T_d$  is the delay spread. The delay spread is the largest difference in propagation time between the longest and shortest path defined as

$$T_d = \max_{i,j} |\tau_{d_i} - \tau_{d_j}|, \quad (3.9)$$

with  $\tau_{d_i}$  being the delay of  $i$ -th path. In case that the coherence bandwidth  $W_c$  is considerably larger than the bandwidth of the system, the channel is said to be flat fading. If, on the other hand, the coherence bandwidth is much smaller than the bandwidth of the system then the channel is called frequency selective.

### 3.1.1 Selection of the modulation scheme

In order to decide which modulation scheme is better suited for frequency selective LTI channels, both, the frequency first and the time first modulation scheme, are simulated in an ITU PedB channel [13]. Note that the 95% confidence intervals are plotted in gray color. The BER curves shown in Figure 3.1 indicate that for frequency selective channels it is better to use the frequency first modulation scheme since the BER is smaller than for the time first modulation scheme. Furthermore, the induced error floor is smaller. This can also be verified by the uncoded throughput curves shown in Figure 3.2. The throughput with the frequency first modulation scheme is higher than with the time first modulation scheme.

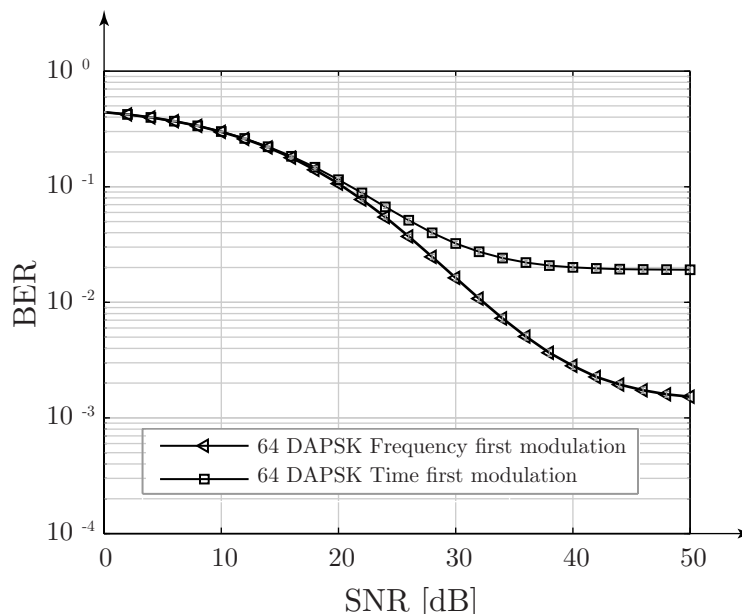


Figure 3.1: BER of the frequency first modulation scheme compared to the time first modulation scheme with 64-DAPSK in an ITU PedB channel

This behavior can be explained by taking a closer look at the modulation schemes. As stated in Equation (2.21) a variation of the channel can introduce additional errors in the quantization process, irrespective of the noise. In

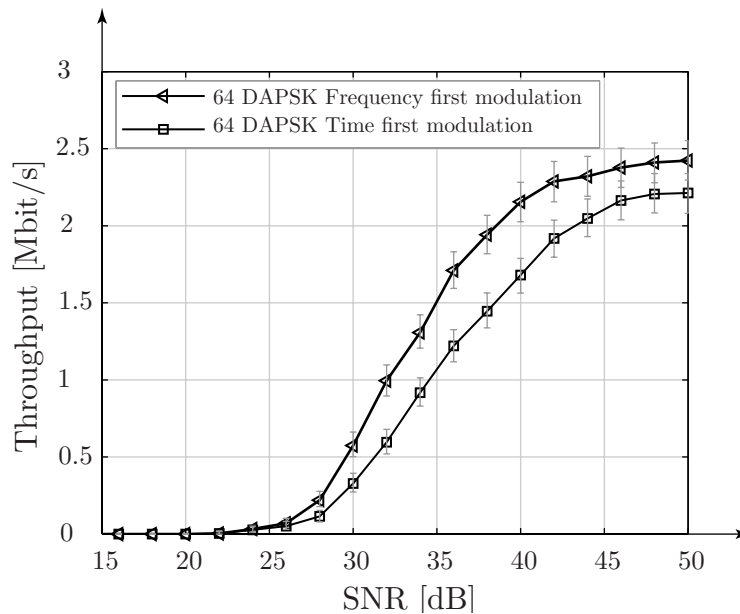


Figure 3.2: Uncoded throughput of the frequency first modulation scheme compared to the time first modulation scheme with 64-DAPSK in an ITU PedB channel

the frequency first modulation scheme the modulation starts with modulating the first 11 information symbols in the frequency direction, which is followed by modulating the rest of the information symbols in the time direction (see Section 2.3). In the detection process, the variation of the channel is only effective while detecting in the frequency direction, since the channel stays constant in the time direction. Compared to that, in the time first modulation scheme the differential modulation starts with modulating the first 13 information symbols in the time direction, which is followed by modulating the rest of the information symbols in the frequency direction. Thus, in the detection process the frequency selectivity of the channel is effective on each OFDM symbol. This leads to the increased BER and residual bit error floor shown in Figure 3.1. Therefore, for the following simulations in this chapter the frequency first modulation scheme is applied. In the next simulation results the performance of differential modulation is presented for different channel types.

### 3.1.2 Uncoded BER and throughput for different channels

Figure 3.3 shows the BER of noncoherent detection compared to coherent detection in an AWGN channel. It can be seen that coherent detection outperforms noncoherent detection with each symbol alphabet size. The performance

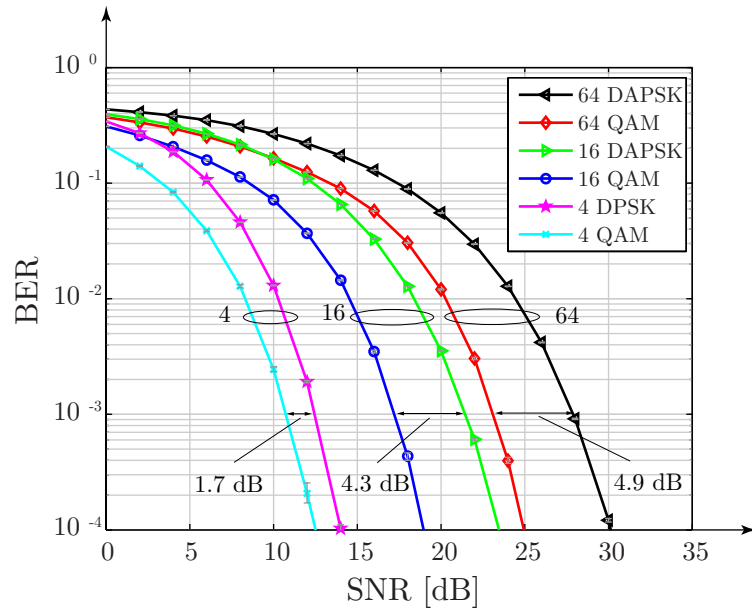


Figure 3.3: BER of noncoherent detection compared to coherent detection in an AWGN channel

difference at a BER of  $10^{-3}$  is approximately 1.7 dB for 4-DPSK compared to 4-QAM. For 16-DAPSK the difference is approximately 4.3 dB compared to 16-QAM and 4.9 dB for 64-DAPSK compared to 64-QAM.

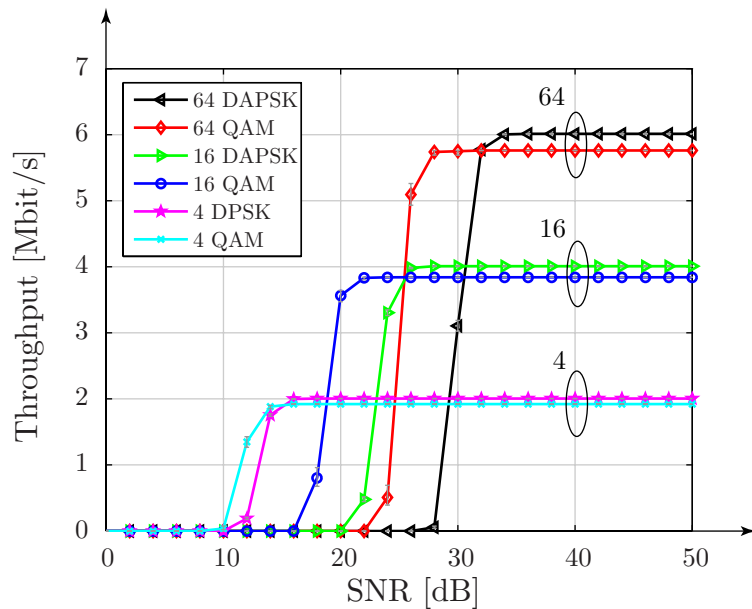


Figure 3.4: Throughput of noncoherent detection compared to coherent detection in an AWGN channel

The uncoded throughput ( $R = 1$ ) in AWGN is presented in Figure 3.4. The

simulation results show that in high SNR regions the maximum throughput of noncoherent detection is higher than that of coherent detection, e.g., the maximum throughput with 64-DAPSK is 6.012 Mbit/s, whereas the maximum throughput with 64-QAM is 5.76 Mbit/s. This amounts to a 4.37 % higher peak throughput, which complies to the result calculated in Equation (2.13). However, the disadvantage of differential modulation is that for the same throughput a higher SNR is required.

In the next simulations differential modulation is considered in an ITU PedB channel. As already discussed before, a frequency selective channel causes an error floor, which decreases the performance of the system. The BER curves in Figure 3.5 indicate that the error floor depends on the alphabet size. The larger the alphabet size is, the higher is the induced error floor. For example, in 64-DAPSK the error floor occurs at a BER of  $1.5 \times 10^{-3}$ , whereas in 16-DAPSK the error floor is at  $0.5 \times 10^{-3}$ . Note, that also coherent detection causes an error floor in a PedB channel. This can be explained by the inaccuracy of the channel estimates caused by the linear interpolation between the estimation positions. As it can be seen from the simulation results, the error floor in coherent detection is smaller than the error floor in noncoherent detection.

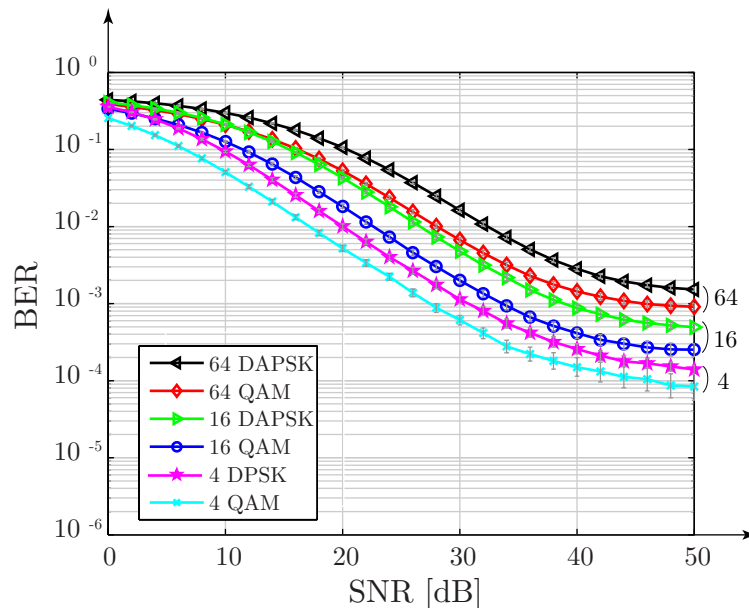


Figure 3.5: BER of noncoherent detection compared to coherent detection in an ITU PedB channel

The corresponding uncoded throughput curves are presented in Figure 3.6. It can be noticed that, compared to an AWGN channel, a frequency selective

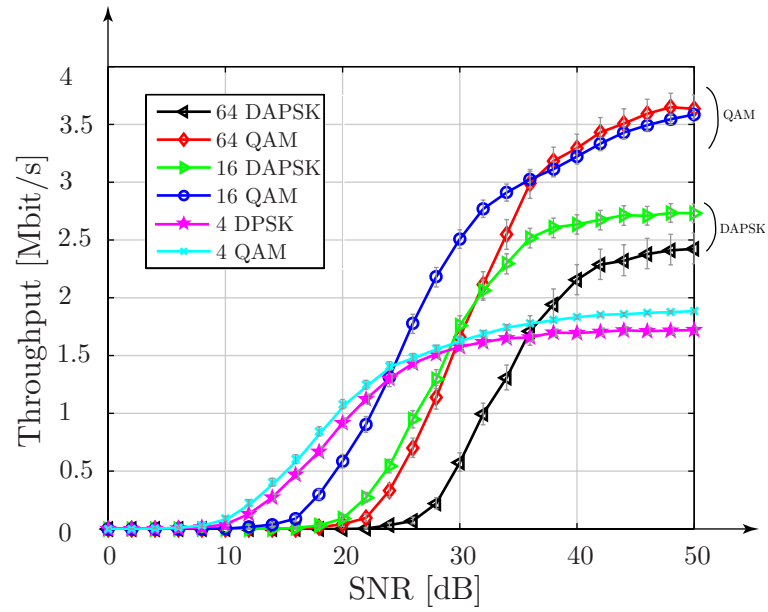


Figure 3.6: Throughput of noncoherent detection compared to coherent detection in an ITU PedB channel

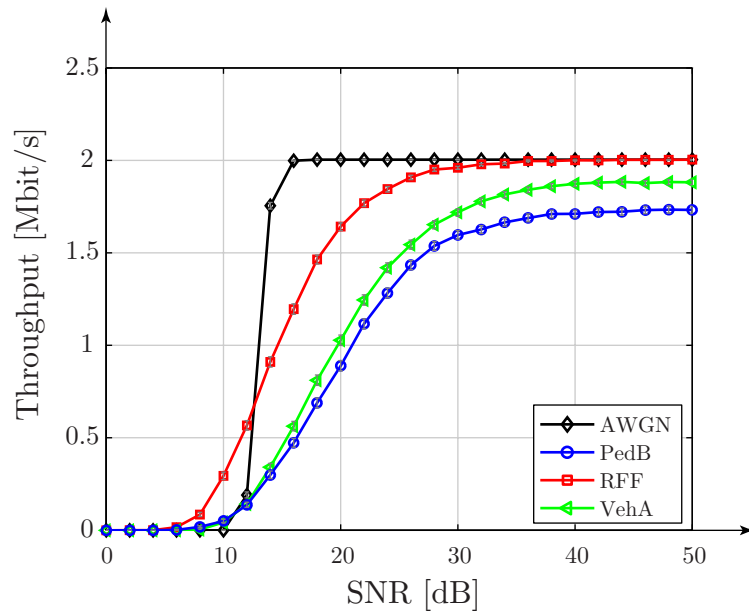


Figure 3.7: Throughput of 4-DPSK in different channels

channel leads to a loss in maximum possible throughput both for coherent and noncoherent detection. The relative loss in throughput is higher with noncoherent detection. For example, with 64-DAPSK the maximum throughput in AWGN is 6.012 Mbit/s, whereas it is only 2.6 Mbit/s in a PedB channel. Compared to that, the maximum throughput for 64-QAM is 5.76 Mbit/s in

AWGN, while the throughput in PedB is 4 Mbit/s. This effect can also be seen with smaller alphabet sizes, however, with the tendency that the relative throughput loss decreases with smaller alphabet size. Furthermore, for the uncoded throughput in PedB 16-DAPSK outperforms 64-DAPSK, since for the same throughput a lower SNR is required. The reason for that behavior is that in 64-DAPSK the phase detection regions are smaller than in 16-DAPSK, which means that a variation of the channel leads easier to a phase error.

Figure 3.7 shows the uncoded throughput of 4-DPSK for channels with different delay spreads. The loss of uncoded throughput compared to the AWGN channel depends on the delay spread of the channel. For example, in a Rayleigh flat fading (RFF) channel, noncoherent detection is able to achieve the same peak throughput as in AWGN, since the RFF channel is not frequency selective. Compared to that, frequency selective ITU PedB and ITU VehA channels lead to a decrease of throughput. The delay spread of the ITU PedB channel is greater than that of the ITU VehA channel [13, Table 2]. Therefore, the throughput of the ITU PedB channel is lower than the throughput of the ITU VehA channel. Thus, if the frequency selectivity of the channel is too large, in the uncoded case, the originally offered higher possible peak throughput of 4.73% of noncoherent detection cannot be achieved.

### 3.1.3 Coded throughput in an ITU PedB channel

Figure 3.8 shows the coded throughput of coherent and noncoherent detection in an ITU PedB channel. The modulation scheme and coding rate  $R$  are adapted according to the current CQI. An overview of the modulation schemes and the corresponding coding rates is presented in Table 3.1. The coded throughput is obtained by determining the maximum throughput at each SNR point and each subframe over all CQIs and averaging it over the number of simulated subframes. Since the conventional noncoherent detection scheme does not offer soft information in the decoding process, out of fairness for the comparison, the soft information of the coherent detection was not utilized either. As it can be seen from the graph, coherent detection outperforms noncoherent detection in terms of coded throughput. The simulation results reveal that the loss of noncoherent detection to coherent detection is about 3 dB at a throughput of 1 Mbit/s and increases to about 3.8 dB at a throughput of 4 Mbit/s. Furthermore, the potential throughput gain of noncoherent detection is only achieved at a very high SNR of at least 34.5 dB, which is not realistic for wireless transmission systems.



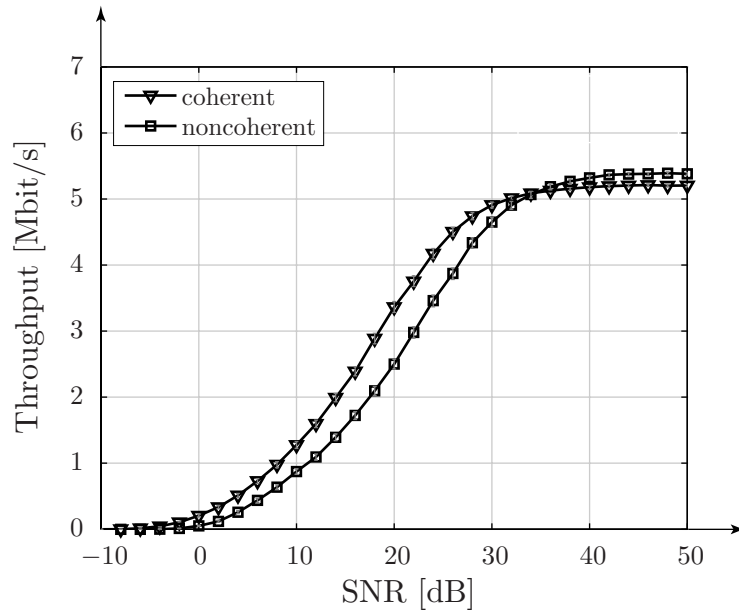


Figure 3.8: Coded throughput in PedB

CQI	Modulation scheme	Coding rate
1	4QAM, 4DPSK	0.076
2	4QAM, 4DPSK	0.117
3	4QAM, 4DPSK	0.189
4	4QAM, 4DPSK	0.301
5	4QAM, 4DPSK	0.439
6	4QAM, 4DPSK	0.588
7	16QAM, 16DAPSK	0.369
8	16QAM, 16DAPSK	0.479
9	16QAM, 16DAPSK	0.602
10	64QAM, 64DAPSK	0.455
11	64QAM, 64DAPSK	0.554
12	64QAM, 64DAPSK	0.650
13	64QAM, 64DAPSK	0.754
14	64QAM, 64DAPSK	0.853
15	64QAM, 64DAPSK	0.926

Table 3.1: CQI with corresponding modulation and coding scheme

### 3.2 Multiple Symbol Differential Detection

As demonstrated in Section 3.1, noncoherent detection suffers from a performance loss compared to coherent detection that depends on the alphabet size  $M$ . Furthermore, it introduces an error floor that cannot be omitted by conventional noncoherent detection techniques. A solution to the performance loss was proposed by Divsalar et al. with multiple symbol differential detection (MSDD) [18]. The basic idea is to process blocks of  $N$  data symbols to jointly detect  $N - 1$  information symbols. In [19], Ho et. al. demonstrated, that by exploiting knowledge about the correlation statistics of the channel in the detection process, the performance can be effectively improved. Furthermore, for frequency selective channels the error floor can be reduced or even eliminated. In the following mathematical description, MSDD is considered in the frequency direction, following the derivations in [19]. For the sake of simplicity of notation the OFDM symbol index  $n$  is omitted. A vector of  $N$  received data symbols is called observation window. After detecting the  $N - 1$  information symbols out of the  $N$  received data symbols, the observation window moves on by  $N - 1$  symbol positions. This leads to an overlap of one data symbol between consecutive windows. An illustration is shown in Figure 3.9. For the following derivation  $M$ -PSK is assumed as symbol alphabet.

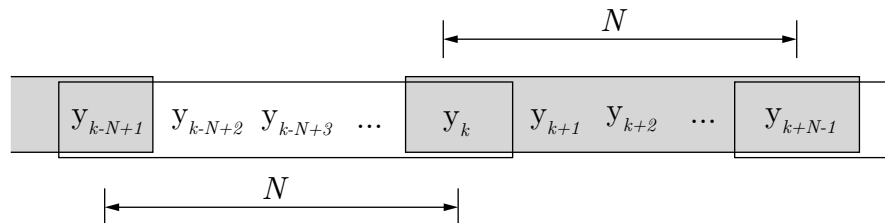


Figure 3.9: Multiple symbol detection in frequency direction

The received symbol vector  $\mathbf{y} = (y_k, y_{k+1}, \dots, y_{k+N-1})^T$  can be written in vector-matrix form as

$$\mathbf{y} = \mathbf{X}\mathbf{h} + \mathbf{v}, \quad (3.10)$$

with

$$\mathbf{X} = \begin{pmatrix} x_k & 0 & \cdots & 0 \\ 0 & x_{k+1} & & \vdots \\ \vdots & & \ddots & 0 \\ 0 & \cdots & 0 & x_{k+N-1} \end{pmatrix}, \quad (3.11)$$

$$\mathbf{h} = (H_k, H_{k+1}, \cdots, H_{k+N-1})^T, \quad (3.12)$$

and

$$\mathbf{v} = (v_k, v_{k+1}, \cdots, v_{k+N-1})^T. \quad (3.13)$$

Due to the differential modulation process, the data symbol  $x_k = x_{k-1}d_k$  (see Equation (2.1)) can be calculated as

$$x_k = x_1 p_k, \quad (3.14)$$

with

$$p_k = \prod_{j=2}^k d_j. \quad (3.15)$$

This allows to rewrite Equation (3.10) as

$$\mathbf{y} = x_1 p_k \mathbf{Z} \mathbf{h} + \mathbf{v},$$

with

$$\mathbf{Z} = \begin{pmatrix} 1 & 0 & \cdots & 0 \\ 0 & z_{k+1} & & \vdots \\ \vdots & & \ddots & 0 \\ 0 & \cdots & 0 & z_{k+N} \end{pmatrix}, \quad (3.16)$$

and

$$z_m = \prod_{l=k+1}^m d_l, \quad m = k+1, \cdots, k+N \quad (3.17)$$

The received vector  $\mathbf{y}$  is input to a maximum likelihood sequence estimator

---

(MLSE). The MLSE searches for the most likely transmitted sequence of information symbols  $\hat{\mathbf{d}} = (\hat{d}_{k+1}, \hat{d}_{k+2}, \dots, \hat{d}_{N-1})$  of length  $N - 1$ , i.e., the one that maximizes the conditional probability density function [19]

$$p(\mathbf{y}|\mathbf{d}) = \frac{\exp(-\mathbf{y}^H \mathbf{R}_{\mathbf{y}\mathbf{y}}^{-1} \mathbf{y})}{\pi^N \det(\mathbf{R}_{\mathbf{y}\mathbf{y}})}. \quad (3.18)$$

Thus

$$\begin{aligned} \hat{\mathbf{d}} &= \operatorname{argmax}_{\mathbf{d} \in \mathcal{D}^{N-1}} \{p(\mathbf{y}|\mathbf{d})\} \\ &= \operatorname{argmax}_{\mathbf{d} \in \mathcal{D}^{N-1}} \left\{ \frac{\exp(-\mathbf{y}^H \mathbf{R}_{\mathbf{y}\mathbf{y}}^{-1} \mathbf{y})}{\pi^N \det(\mathbf{R}_{\mathbf{y}\mathbf{y}})} \right\}. \end{aligned} \quad (3.19)$$

Here,  $\mathbf{R}_{\mathbf{y}\mathbf{y}}$  is the autocorrelation matrix of the received data symbol vector conditioned on the transmitted information symbol vector  $\mathbf{d}$  and  $\mathcal{D}$  is the symbol alphabet for  $M$ -PSK. Under the assumption that the sequence  $\mathbf{d}$  was transmitted and the power of  $x_1$  and  $z_k$  is 1,  $\mathbf{R}_{\mathbf{y}\mathbf{y}}$  can be calculated as

$$\begin{aligned} \mathbf{R}_{\mathbf{y}\mathbf{y}} &= E\{\mathbf{y}\mathbf{y}^H | \mathbf{d}\} = E\{(x_1 p_k \mathbf{Z}\mathbf{h} + \mathbf{v})(x_1 p_k \mathbf{Z}\mathbf{h} + \mathbf{v})^H | \mathbf{d}\} \\ &= \mathbf{Z} E\{\mathbf{h}\mathbf{h}^H\} \mathbf{Z}^H + \sigma_v^2 \mathbf{I}_N, \end{aligned} \quad (3.20)$$

where  $\mathbf{I}_N$  is an  $N \times N$  identity matrix. In Equation (3.20) we used the fact that  $\mathbf{Z}$  becomes deterministic, if it is conditioned on  $\mathbf{d}$ , and the noise  $\mathbf{v}$  is assumed to be i.i.d. zero mean. With an  $M$ -PSK alphabet,  $\mathbf{Z}$  is unitary, i.e.,  $\mathbf{Z}^{-1} = \mathbf{Z}^H$  and therefore Equation (3.20) can be written as

$$\mathbf{R}_{\mathbf{y}\mathbf{y}} = \mathbf{Z}(\boldsymbol{\Sigma}_{\mathbf{h}\mathbf{h}} + \sigma_v^2 \mathbf{I}_N) \mathbf{Z}^H, \quad (3.21)$$

with  $\boldsymbol{\Sigma}_{\mathbf{h}\mathbf{h}} = E\{\mathbf{h}\mathbf{h}^H\}$  being the autocorrelation matrix of the channel. For  $M$ -PSK the determinant of  $\mathbf{R}_{\mathbf{y}\mathbf{y}}$  is constant and independent of  $\mathbf{Z}$ . This applies, since for square matrices

$$\begin{aligned}
\det(\mathbf{ABC}) &= \det(\mathbf{A})\det(\mathbf{B})\det(\mathbf{C}) \\
&= \det(\mathbf{B})\det(\mathbf{C})\det(\mathbf{A}) \\
&= \det(\mathbf{BCA})
\end{aligned} \tag{3.22}$$

and therefore

$$\begin{aligned}
\det(\mathbf{R}_{\mathbf{yy}}) &= \det(\mathbf{Z}(\boldsymbol{\Sigma}_{\mathbf{hh}} + \sigma_v^2 \mathbf{I}_N) \mathbf{Z}^H) \\
&= \det((\boldsymbol{\Sigma}_{\mathbf{hh}} + \sigma_v^2 \mathbf{I}_N) \mathbf{Z}^H \mathbf{Z}) \\
&= \det((\boldsymbol{\Sigma}_{\mathbf{hh}} + \sigma_v^2 \mathbf{I}_N) \mathbf{Z}^{-1} \mathbf{Z}) \\
&= \det(\boldsymbol{\Sigma}_{\mathbf{hh}} + \sigma_v^2 \mathbf{I}_N)
\end{aligned} \tag{3.23}$$

Thus, Equation (3.19) can be rewritten as

$$\begin{aligned}
\hat{\mathbf{d}} &= \underset{\mathbf{d} \in \mathcal{D}^{N-1}}{\operatorname{argmin}} \{ \mathbf{y}^H \mathbf{R}_{\mathbf{yy}}^{-1} \mathbf{y} \} \\
&= \underset{\mathbf{d} \in \mathcal{D}^{N-1}}{\operatorname{argmin}} \{ (\mathbf{y}^H \mathbf{Z}) (\boldsymbol{\Sigma}_{\mathbf{hh}} + \sigma_v^2 \mathbf{I}_N)^{-1} (\mathbf{Z}^H \mathbf{y}) \}.
\end{aligned} \tag{3.24}$$

The MLSE searches for the information symbol sequence  $\hat{\mathbf{d}}$  in all possible symbol sequences  $\mathbf{d}$  that minimizes Equation (3.24). This is dependent on the autocorrelation of the channel. If the detection is performed in frequency direction,  $\boldsymbol{\Sigma}_{\mathbf{hh}}$  describes the correlation between subcarriers. In an LTI channel it can be calculated as [20]

$$\boldsymbol{\Sigma}_{\mathbf{hh}}^{(f)} = \mathbf{W} E \{ \mathbf{g} \mathbf{g}^H \} \mathbf{W}^H = \mathbf{W} \mathbf{H}_{PDP} \mathbf{W}^H, \tag{3.25}$$

where  $\mathbf{W}$  is a  $K \times K$  DFT matrix and  $K$  stands for the size of the DFT. The superscript  $f$  indicates that the autocorrelation is considered in the frequency direction and the vector  $\mathbf{g}$  represents the current realization of the channel in the time domain. The matrix  $\mathbf{H}_{PDP}$  is of size  $K \times K$  and has the coefficients of the power delay profile (PDP) on its diagonal. The PDP is of length  $L$ . In practical realizations neither the length  $L$  nor the shape of the PDP is known to receiver. For the simulations, an exponential PDP with fixed length  $L$  is

assumed at the receiver. The decay constant is set to one.

Unfortunately the complexity of multiple symbol differential detection increases exponentially with the size of the observation window  $N$ , if a brute-force search is applied. The next Section 3.3 describes how the complexity can be reduced with the help of sphere decoding.

### 3.3 Multiple Symbol Differential Sphere Decoding

The concept of applying sphere decoding (SD) to multiple symbol differential detection was introduced by Lampe et al. in [21]. It originates from an adaption of a common coherent detection problem in MIMO, where the task is to find a vector  $\hat{\mathbf{x}}$  that solves the following optimization problem

$$\hat{\mathbf{x}} = \underset{\mathbf{x}}{\operatorname{argmin}} \|\mathbf{y} - \mathbf{H}\mathbf{x}\|^2. \quad (3.26)$$

In this context  $\mathbf{x}$  is a vector of transmitted data symbols of length  $N_s$ ,  $\mathbf{H}$  is an  $(N_s \times N_r)$ -dimensional channel matrix,  $\mathbf{y}$  is the received vector of length  $N_r$ , and  $N_s$  and  $N_r$  represent the number of transmit and receive antennas, respectively. If  $\mathbf{H}$  is known to the receiver this can be rewritten as [22]

$$\hat{\mathbf{x}} = \underset{\mathbf{x}}{\operatorname{argmin}} \|\mathbf{U}(\mathbf{x} - \mathbf{x}_{LS})\|^2, \quad (3.27)$$

where  $\mathbf{U}$  is an upper triangular matrix that is obtained by the Cholesky factorization  $\mathbf{H}^H\mathbf{H} = \mathbf{U}^H\mathbf{U}$ , and  $\mathbf{x}_{LS}$  is the LS solution. It can be shown that this problem is similar to finding the shortest vector in a lattice, which can effectively be solved with the SD algorithm. The SD algorithm reduces the complexity of the search [22].

In [21], Lampe et al. found that the joint maximum likelihood (ML) detection of  $N - 1$  differentially transmitted information symbols out of  $N$  received data symbols can be modeled as the detection problem of the previously discussed MIMO case by setting  $N_s = N - 1$  and  $N_r = N$ . By using the Cholesky factorization on the channel statistics it is possible to find a similar decision metric as in Equation (3.27) on which SD can be applied. The following mathematical description is analogous to that shown in Section 3.2 and follows the derivations in [21]. The difference to the previous derivation is that  $\mathbf{d}$  is changed to  $\mathbf{x}$ . The ML decision rule for the transmitted data vector  $\hat{\mathbf{x}}$  with the conditional density function

$$p(\mathbf{y}|\mathbf{x}) = \frac{\exp(-\mathbf{y}^H \mathbf{R}_{\mathbf{y}\mathbf{y}}^{-1} \mathbf{y})}{\pi^N \det(\mathbf{R}_{\mathbf{y}\mathbf{y}})}, \quad (3.28)$$

can be written as

$$\begin{aligned} \hat{\mathbf{x}} &= \operatorname{argmax}_{\mathbf{x} \in \mathcal{X}^N} \{p(\mathbf{y}|\mathbf{x})\} \\ &= \operatorname{argmax}_{\mathbf{x} \in \mathcal{X}^N} \left\{ \frac{\exp(-\mathbf{y}^H \mathbf{R}_{\mathbf{y}\mathbf{y}}^{-1} \mathbf{y})}{\pi^N \det(\mathbf{R}_{\mathbf{y}\mathbf{y}})} \right\}, \end{aligned} \quad (3.29)$$

where  $\mathbf{R}_{\mathbf{y}\mathbf{y}}$  is the autocorrelation matrix of the received data vector  $\mathbf{y}$  conditioned on the transmitted data vector  $\mathbf{x}$ . Similarly to Equation (3.20) it can be calculated as

$$\mathbf{R}_{\mathbf{y}\mathbf{y}} = \mathbf{X} E\{\mathbf{h}\mathbf{h}^H\} \mathbf{X}^H + \sigma_v^2 \mathbf{I}_N \quad (3.30)$$

$$= \mathbf{X} (E\{\mathbf{h}\mathbf{h}^H\} + \sigma_v^2 \mathbf{I}_N) \mathbf{X}^H, \quad (3.31)$$

where again the fact was used that  $\mathbf{X}$  is unitary for an  $M$ -PSK symbol alphabet. Thus Equation (3.29) can be rewritten as

$$\hat{\mathbf{x}} = \operatorname{argmin}_{\mathbf{x} \in \mathcal{X}^N} \{\mathbf{y}^H \mathbf{R}_{\mathbf{y}\mathbf{y}}^{-1} \mathbf{y}\}. \quad (3.32)$$

With

$$\mathbf{R}_{\mathbf{y}\mathbf{y}} = \operatorname{diag}\{\mathbf{x}\} \mathbf{C} \operatorname{diag}\{\mathbf{x}^*\}, \quad (3.33)$$

$$\mathbf{C} \triangleq \Sigma_{\mathbf{h}\mathbf{h}} + \sigma_v^2 \mathbf{I}_N, \quad (3.34)$$

$$\operatorname{diag}\{\mathbf{x}^*\} \mathbf{y} = \operatorname{diag}\{\mathbf{y}\} \mathbf{x}^*, \quad (3.35)$$

where  $(\cdot)^*$  denotes the (componentwise) complex conjugate, Equation (3.32)

can be rewritten as

$$\hat{\mathbf{x}} = \underset{\mathbf{x} \in \mathcal{X}^N}{\operatorname{argmin}} \{(\operatorname{diag}\{\mathbf{y}\}\mathbf{x}^*)^H \mathbf{C}^{-1}(\operatorname{diag}\{\mathbf{y}\}\mathbf{x}^*)\}. \quad (3.36)$$

The expression above is a quadratic form in  $\mathbf{x}$ . By using the the Cholesky factorization of the inverse matrix

$$\mathbf{C}^{-1} = \mathbf{L}\mathbf{L}^H \quad (3.37)$$

and defining

$$\mathbf{U} \triangleq (\mathbf{L}^H \operatorname{diag}\{\mathbf{y}\})^*, \quad (3.38)$$

where  $\mathbf{L}$  and  $\mathbf{U}$  are lower and an upper triangular matrices, respectively, Equation (3.36) can finally be written as

$$\hat{\mathbf{x}} = \underset{\mathbf{x} \in \mathcal{X}^N}{\operatorname{argmin}} \{||\mathbf{U}\mathbf{x}||^2\}. \quad (3.39)$$

This decision rule is equal to Equation (3.27), if the vector  $\mathbf{x}_{LS}$  is set to the all zero vector. This means that the ML-MSDD can be regarded as a shortest vector problem. Thus, to find the most likely transmitted data symbol vector  $\hat{\mathbf{x}}$  out of all possible data symbol vectors  $\mathbf{x}$ , the SD algorithm can be applied. This is referred to as multiple symbol differential sphere decoding (MSDSD). With the relation in Equation (2.1) we obtain  $\hat{\mathbf{d}}$  which is decoded to  $(N-1) \cdot p$  information bits according to Section 2.1.

For  $N = 2$ , in  $M$ -PSK the detection process presented in Equation (2.7) becomes equivalent to the ML decision rule presented in Equation (3.32). This means that the simple noncoherent detection process is ML optimal for  $N = 2$ . The complexity reduction of the SD algorithm comes from limiting the search for possible candidate vectors  $\mathbf{x}$  to those that lie inside a sphere of radius  $\lambda$ ,

$$||\mathbf{U}\mathbf{x}||^2 \leq \lambda^2. \quad (3.40)$$

Since  $\mathbf{U}$  is an upper triangular matrix the condition in Equation (3.40) can be checked component by component. That means, after having found a (preliminary) decision  $\hat{x}_l$  for the last  $N - i$  components  $x_l$ , with  $i + 1 \leq l \leq N$ , a



condition for the  $i$ -th component  $x_i$ , with  $1 \leq i \leq N$ , is obtained. To make that clearer, let us introduce the squared length  $d_{i+1}^2$  as [21]

$$d_{i+1}^2 = \sum_{l=i+1}^N \left| \sum_{j=l}^N u_{lj} \hat{x}_j \right|^2, \quad (3.41)$$

that accounts for the length of the last  $N - i$  components. Here,  $u_{ij}$  denotes  $i$ -th row and  $j$ -th column element of  $\mathbf{U}$  and  $\hat{x}_j$  is a possible solution for the  $j$ -th data symbol of the vector  $\mathbf{x}$ . Then, possible solutions for the data symbol  $x_i$  have to satisfy the criterion [21]

$$d_i^2 = \left| u_{ii}x_i + \sum_{j=i+1}^N u_{ij}\hat{x}_j \right|^2 + d_{i+1}^2 \leq \lambda^2. \quad (3.42)$$

For a low complexity of the SD algorithm it is critical to order the possible candidate symbols  $x_i$ . In [21] the Schnorr-Euchner [23] algorithm is applied. The symbols  $x_i$  are ordered according to the length  $d_i$ , starting with the smallest one. Thus, the search for a candidate symbol  $x_i$  can already be terminated, if the current length  $d_i$  exceeds the sphere radius  $\lambda$ . A detailed description on how to implement the SD algorithm can be found in [21, 24].

The MSDSD metric is invariant to a common phase shift of the components of vector  $\mathbf{x}$ . Thus, the detected information symbol vector  $\hat{\mathbf{d}}$  is invariant to such a common phase shift. This degree of freedom can be exploited to set the last data symbol  $x_N = 1$  and reduce the ML-search to the remaining  $N - 1$  data symbols.

Unfortunately, the SD algorithm cannot directly be applied to non constant modulus alphabets like APSK, since in this case the matrix  $\mathbf{X}$  in Equation (3.30) is not unitary anymore. The metric in Equation (3.29) depends on the transmitted amplitudes of the data symbols. In order to circumvent that problem, let us rewrite the data symbol matrix  $\mathbf{X}$  with Equation (2.3) as

$$\mathbf{X} = \mathbf{A}\mathbf{S} \quad (3.43)$$

where  $\mathbf{A} = \text{diag}\{\mathbf{a}\}$ ,  $\mathbf{S} = \text{diag}\{\mathbf{s}\}$  and  $\mathbf{a}$  and  $\mathbf{s}$  are size  $N$  amplitude symbol and phase symbol vectors, respectively.

Thus the autocorrelation matrix  $\mathbf{R}_{\mathbf{y}\mathbf{y}}$  in Equation (3.30) can be written as

$$\begin{aligned}
\mathbf{R}_{\mathbf{y}\mathbf{y}} &= \mathbf{X}\boldsymbol{\Sigma}_{\mathbf{h}\mathbf{h}}\mathbf{X}^H + \sigma_v^2\mathbf{I}_N \\
&= \mathbf{A}\mathbf{S}\boldsymbol{\Sigma}_{\mathbf{h}\mathbf{h}}(\mathbf{A}\mathbf{S})^H + \sigma_v^2\mathbf{I}_N \\
&= \mathbf{S}(\tilde{\boldsymbol{\Sigma}}_{\mathbf{h}\mathbf{h}} + \sigma_v^2\mathbf{I}_N)\mathbf{S}^H,
\end{aligned} \tag{3.44}$$

with

$$\tilde{\boldsymbol{\Sigma}}_{\mathbf{h}\mathbf{h}} = \mathbf{A}\boldsymbol{\Sigma}_{\mathbf{h}\mathbf{h}}\mathbf{A}^H. \tag{3.45}$$

Since  $\mathbf{S}$  is unitary again the SD algorithm can be applied to detect the phase vector  $\mathbf{s}$  of the transmitted data vector  $\mathbf{x}$ . With the notations of Equation (3.33) to Equation (3.38), changing  $\mathbf{x}$  to  $\mathbf{s}$ , we arrive at the joint detection process of the data amplitude vector  $\mathbf{a}$  and data phase vector  $\mathbf{s}$  by [9]

$$\hat{\mathbf{x}} = \hat{\mathbf{a}}^T \cdot \hat{\mathbf{s}} = \underset{\mathbf{a} \in \mathcal{A}^N, \mathbf{s} \in \mathcal{S}^N}{\operatorname{argmin}} \left\{ \frac{\|\mathbf{U}\mathbf{s}\|^2}{\det(\mathbf{R}_{\mathbf{y}\mathbf{y}})} \right\}. \tag{3.46}$$

In the joint detection process the data amplitude vector  $\mathbf{a}$  is varied inside the symbol alphabet  $\mathcal{A}$  and for each possible choice of  $\mathbf{a}$  the SD algorithm is applied to detect the data phase vector  $\hat{\mathbf{s}}$ . This gives a significant reduction in complexity, since the complexity of the brute force detection comes mainly from the phase detection process. Note, however, that for each variation of the data amplitude vector the inverse of the  $N \times N$  matrix  $\tilde{\mathbf{C}} = \tilde{\boldsymbol{\Sigma}}_{\mathbf{h}\mathbf{h}} + \sigma_v^2\mathbf{I}_N$  has to be calculated. This is not the case for  $M$ -PSK since here  $\mathbf{C}$  stays constant (see Equation (3.34)). With the relations of Equations (2.1) to (2.4) we obtain  $\hat{\mathbf{d}} = \hat{\boldsymbol{\gamma}}^T \cdot \hat{\boldsymbol{\beta}}$ , where  $\hat{\boldsymbol{\gamma}}$  and  $\hat{\boldsymbol{\beta}}$  are size  $N - 1$  estimated amplitude information symbol and phase information symbol vectors, respectively. These vectors are decoded to  $(N - 1) \cdot p$  information bits according to Section 2.1.

The principle of MSDSD can be used both in the frequency and in the time direction. If the detection is performed in the time direction, similar to detection in the frequency direction,  $N$  received data symbols on a subcarrier are used to jointly detect  $N - 1$  information symbols. It is interesting to note that for DPSK the inverse correlation matrix  $\mathbf{C}^{-1}$  in LTI very slowly fading channels can be written as [24]

$$\mathbf{C}^{-1} = -\frac{1}{(N + \sigma_v^2)\sigma_v^2}\mathbf{1}_N + \frac{1}{\sigma_v^2}\mathbf{I}_N, \tag{3.47}$$

where  $\mathbf{1}_N$  is an all ones matrix of size  $N$ . If the channel is frequency flat this matrix can be used for MSDSD in both the frequency and in the time direction. In [24] it is shown that this correlation matrix can also be applied for an AWGN channel.

### 3.3.1 Uncoded BER and throughput with MSDSD

In the following simulations the performance of 4-DPSK with MSDSD is investigated for LTI channels and compared to coherent detection. The simulations are performed with different observation window sizes  $N$  and different channels.

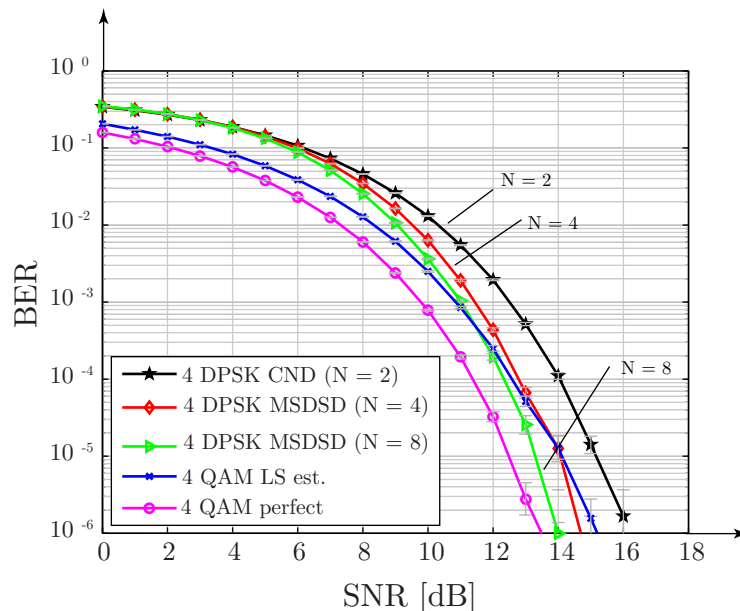


Figure 3.10: BER of 4-DPSK with MSDSD in an AWGN channel

In Figure 3.10 the BER in an AWGN channel is shown. As already presented before at a BER of  $10^{-3}$  the conventional noncoherent detection (CND) with an observation window size of  $N = 2$ , has a loss of about 1.7 dB compared to coherent detection. If the observation window size is increased to  $N = 4$ , this means 3 information symbols are jointly detected out of 4 received data symbols, the gain of MSDSD is about 1 dB compared to the CND. If the observation window is further increased to  $N = 8$  the gain is about 1.6 dB. This means, that in an AWGN channel at a BER of  $10^{-3}$ , coherent detection with LS channel estimation, ZF equalization and linear interpolation between the channel estimation positions, only slightly outperforms MSDSD with an

observation window size of  $N = 8$  by 0.1 dB. If the BER is considered at  $10^{-4}$ , it can be noticed that MSDSD with an observation window of size  $N = 4$  almost achieves the same performance as coherent detection. If the observation window is further increased to  $N = 8$  noncoherent detection outperforms coherent detection by about 0.4 dB.

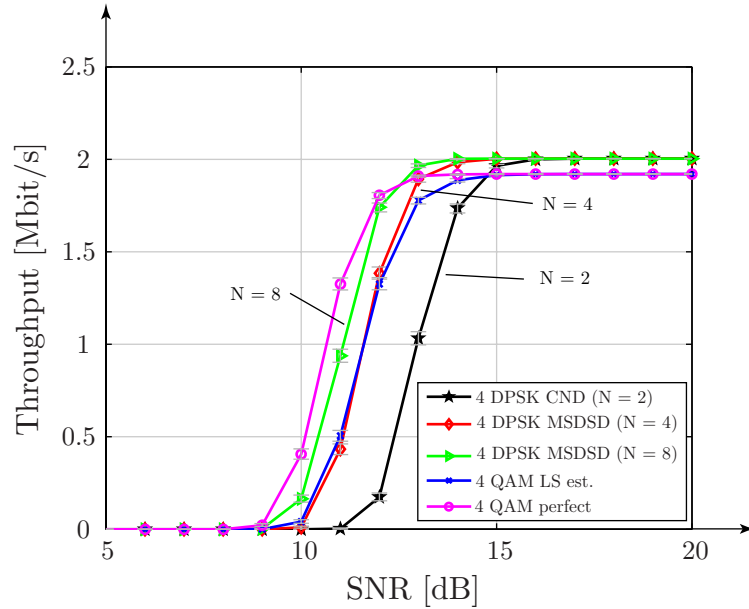


Figure 3.11: Uncoded Throughput of 4-DPSK with MSDSD in an AWGN channel

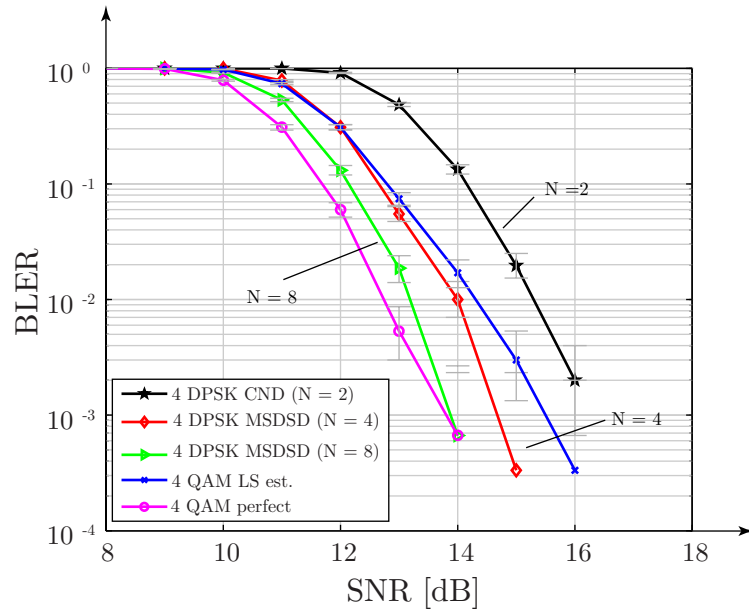


Figure 3.12: BLER of 4-DPSK with MSDSD in an AWGN channel

In Figure 3.11 the uncoded throughput ( $R = 1$ ) of 4-DPSK with MSDSD in

AWGN is presented. The results show that in terms of uncoded throughput coherent detection outperforms CND. If, however, the observation window size  $N$  is increased to 4 or 8, MSDSD starts to outperform coherent detection. In order to explain this behavior, consider the block error rate (BLER) curves shown in Figure 3.12. The BLER is a measure of how many subframes of the total number of transmitted subframes are discarded because of bit errors. These discarded frames do not account for the throughput. The simulations reveal that the BLER of MSDSD is lower than that of CND and coherent detection with LS channel estimation. This is because with MSDSD errors usually occur as error bursts. If one data symbol inside the observation window is detected wrongly, it is likely that also other data symbols inside the observation window are detected wrongly, due to error propagation in the differential detection process. On the other hand, it also may happen that because of MSDSD the whole subframe is detected correctly, where otherwise there would be errors if CND was used. Since the BLER does not depend on the total number of bit errors in a subframe, the BLER of MSDSD is lower than that of CND. The same applies for coherent detection with LS channel estimation. In coherent detection the information symbols are detected independently. This means, that the errors occur more evenly distributed in the subframe. Thus, at a certain SNR it may happen that with MSDSD the whole subframe is detected without any error, while with coherent detection single errors are introduced in the detection process. Therefore, for uncoded transmissions it can happen that with MSDSD the BLER is lower than with coherent detection. This can also be seen from Figure 3.12. Since discarded subframes do not account for the throughput, this leads to the higher throughput of MSDSD with  $N = 8$ . This explanation is also valid for high coding rates  $R$ .

The simulation results in Figure 3.13 present the performance of 4-DPSK with MSDSD in an ITU PedB channel. For the calculation of the correlation matrix  $\Sigma_{\mathbf{H}\mathbf{H}}^{(f)}$  in frequency direction, Equation (3.25) with an exponential PDP of  $L = 8$  was assumed. A closer look at the BER reveals that the performance gain of MSDSD in a PedB channel is less than in an AWGN channel. At a BER of  $10^{-3}$  the gain of MSDSD with  $N = 4$  is about 0.6 dB, with  $N = 8$  the gain is about 0.9 dB, compared to CND. This is because of the smaller correlation of the channel in the frequency direction. A very important simulation result is, that the induced error floor of noncoherent detection in ITU PedB channels can already be effectively mitigated by MSDSD with an observation window size of  $N = 4$ .

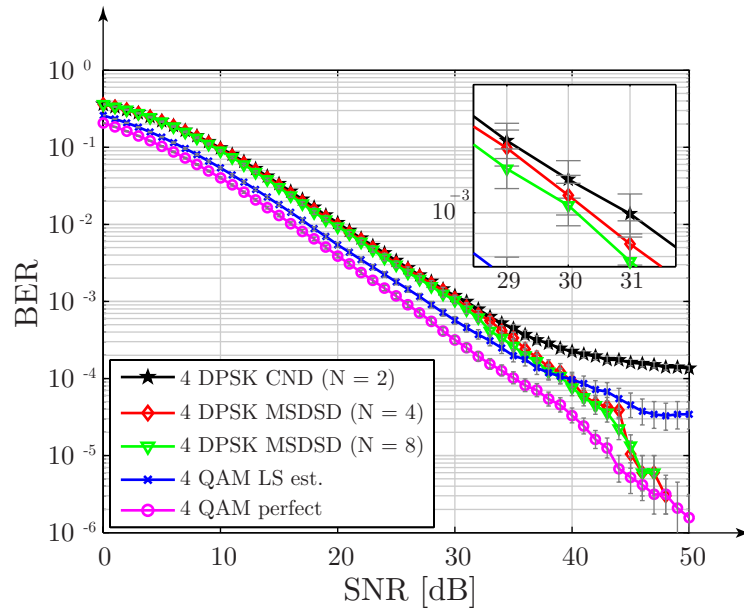


Figure 3.13: BER of 4-DPSK with MSDSD in an ITU PedB channel

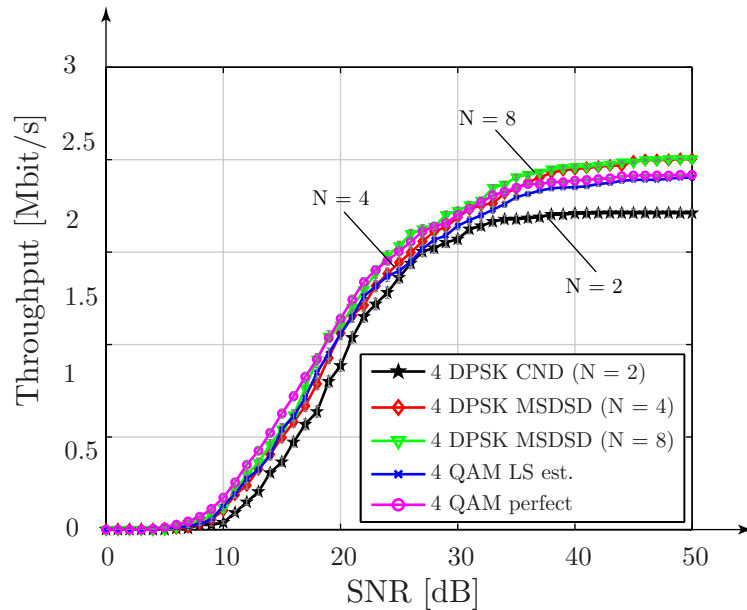


Figure 3.14: Uncoded Throughput of 4-DPSK with MSDSD in ITU PedB

The uncoded throughput of MSDSD in an ITU PedB channel is shown in Figure 3.14. As already discussed in Figure 3.6, frequency selective channels lead to a loss of maximum possible throughput if CND is used. Thus the initially higher offered peak throughput of 4.37 % compared to coherent detection cannot be achieved. If, however, the observation window size is increased to  $N = 4$  or  $N = 8$  this performance loss can be mitigated. Therefore, in the

uncoded case it is possible to omit the reduction of throughput with the help of MSDSD. That behavior can also be observed from the throughput curves.

### 3.3.2 Coded throughput with MSDSD

In the next simulations the coded throughput performance of multiple symbol differential sphere decoding in an AWGN and an ITU PedB channel is compared. Since the detection complexity of DAPSK is still very high, although MSDSD is applied, the maximum observation window length of 16-DAPSK and 64-DAPSK is restricted to  $N = 4$ . For 4-DPSK both an observation window length  $N = 4$  and  $N = 8$  were simulated.

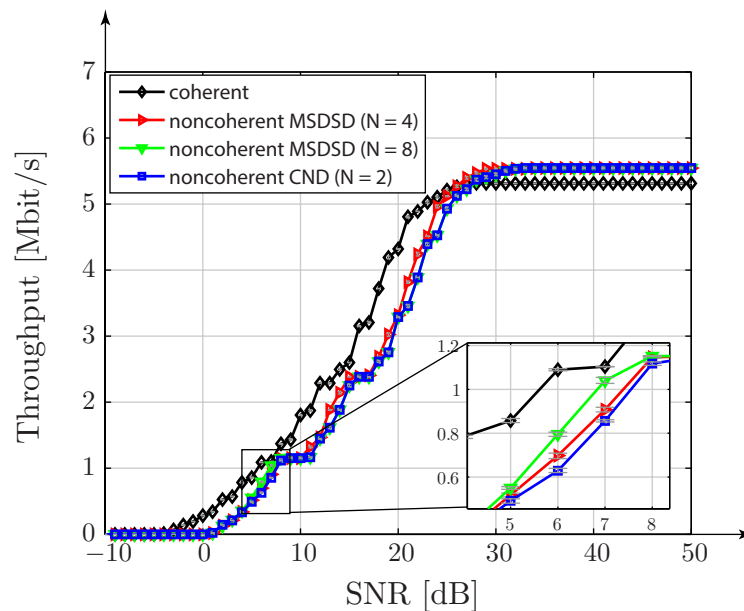


Figure 3.15: Coded Throughput of MSDSD in an AWGN channel

The coded throughput in an AWGN channel is presented in Figure 3.15. A comparison between CND and MSDSD reveals that the gain in coded throughput of MSDSD to CND increases with SNR and observation window size  $N$ . This is because MSDSD in general starts to work better at higher SNR levels (see Figure 3.10). In the low SNR regions (-10 dB to 10 dB) the coded throughput is determined by the 4-DPSK modulation. At a throughput of 0.5 Mbit/s, MSDSD with  $N = 4$  has a gain of 0.15 dB, whereas for  $N = 8$  the gain is 0.3 dB. Compared to that, at a throughput of 1 Mbit/s, MSDSD with  $N = 4$  has a gain of about 0.2 dB and with  $N = 8$  a gain of 0.7 dB,

respectively. If the SNR is increased the coded throughput is determined by 16-DAPSK and 64-DAPSK. Here the same tendency can be observed, that means the performance gain of MSDSD increases with higher SNR. For a throughput of 2 Mbit/s the gain of MSDSD with  $N = 4$  compared to CND is 0.9 dB. At a throughput of 5 Mbit/s MSDSD with  $N = 4$  already gains 1.2 dB compared to CND. Thus, MSDSD is able to improve the performance of noncoherent detection, especially for DAPSK. Nevertheless, coherent detection still outperforms noncoherent detection.

Note, that the coded throughput of coherent detection is higher than that of noncoherent detection, although MSDSD is applied. This is in contradiction to the results presented in Figure 3.11, where it was found that MSDSD with an observation window size of  $N = 8$  achieves a higher throughput than coherent detection. The contradiction can be explained by the effect of coding. As an illustration consider the BLER curves of 4-DPSK and 4-QAM with coding rates  $R$  that correspond to CQI 14 and CQI 15 shown in Figure 3.16. The simulation results show the BLER of 4-DPSK with CND and MSDSD with  $N = 8$ , as well as 4-QAM with coherent detection with LS channel estimation.

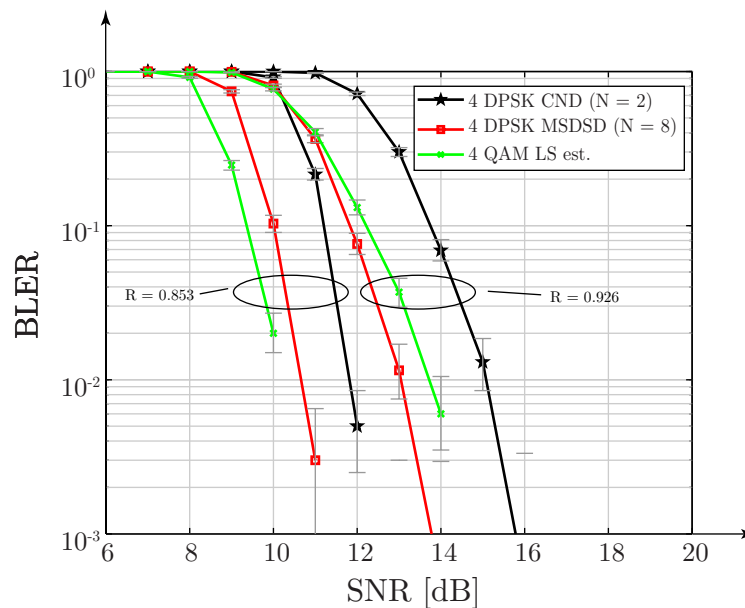


Figure 3.16: 4-DPSK and 4-QAM for  $R = 0.853$  and  $R = 0.926$

As already discussed, errors in MSDSD occur as error bursts, i.e., inside a wrong subframe there are usually a lot of bit errors. On the other hand, due to MSDSD there are also many correctly detected subframes. In coherent detection, bit errors occur more sporadically. Therefore, with coding it is possible to sometimes correct these sporadic errors, while sometimes it is not possible.



The amount of errors that can be corrected depends on the coding rate. The lower  $R$ , the higher is the amount of errors that can be corrected. Thus, for high coding rates  $R$  the BLER of MSDSD with  $N = 8$  is lower than for coherent detection. In this case more subframes can be detected correctly with MSDSD than with coherent detection (see Figure 3.12 and Figure 3.16 for  $R = 0.926$ ). If  $R$  is reduced, coding is able to correct more and more errors. This means, in coherent detection more of the sporadic errors can be corrected, which significantly reduces the BLER. On the other hand, in MSDSD, due to the usually higher amount of errors inside an erroneous subframe, it can happen that coding is not able to correct all the errors. Hence, at a certain  $R$  the BLER of coherent detection becomes lower than that for MSDSD. This can also be seen by the BLER curves in Figure 3.16 for  $R = 0.853$ . Thus, the coded throughput of coherent detection is larger than that of noncoherent detection.

Lastly, it can be observed from Figure 3.15 that the throughput of noncoherent detection in an AWGN channel saturates between about 8 to 10 dB and 15 to 17 dB. At these SNR values the maximum possible throughput of the corresponding symbol alphabet and CQI is already reached. E.g., for 4-DPSK the highest coding rate is  $R = 0.588$ , i.e., CQI = 6 (see Table 3.1). In this case the largest throughput is 1.17 Mbit/s, which corresponds to the flat throughput area between 8 and 10 dB shown in Figure 3.15. Thus, the coding rates specified for coherent detection in LTE are not optimal for noncoherent detection. To omit the saturation, the coding rates need to be adapted. For example the coding rate of CQI 6 could be increased, or the coding rate of CQI 7 could be decreased. The same applies for the saturation area between 15 and 17 dB. Here an adaptation of CQI 9 and CQI 10 in a similar way would be necessary. An exact investigation of how to adapt the coding rates of coherent detection for noncoherent detection was not considered in this thesis.

The last simulation in this chapter presents the coded throughput of MSDSD in an ITU PedB channel, depicted in Figure 3.17. Similar to the AWGN case, the gain of MSDSD compared to CND increases with SNR and observation window size  $N$ . At a throughput of 1 Mbit/s and  $N = 4$  the gain compared to CND is 0.3 dB, whereas the gain for  $N = 8$  is about 0.6 dB. At a throughput of 2 Mbit/s (here already the 16-DAPSK modulation determines the coded throughput) the gain of MSDSD increases to about 0.9 dB. This trend continues with 64-DAPSK. At a throughput of 4 Mbit/s the gain is about 0.9 dB, for 5 Mbit/s it is about 1.2 dB. From the simulation results it can also be

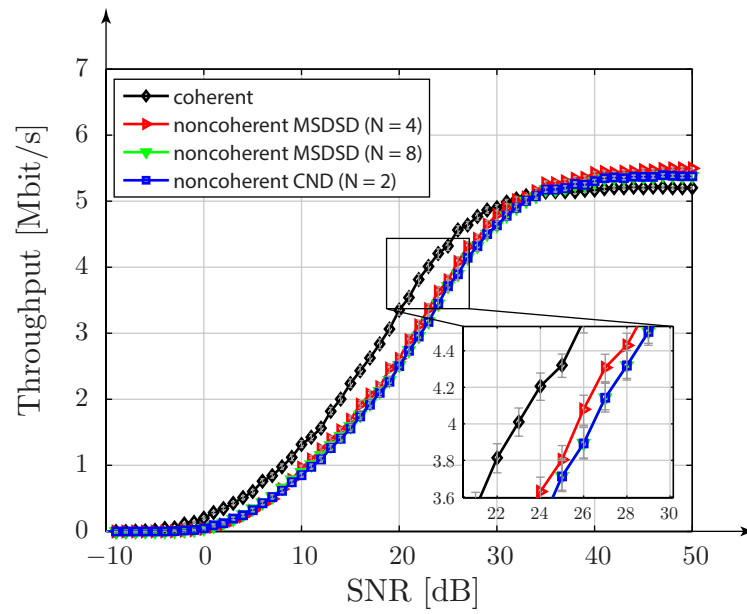


Figure 3.17: Coded Throughput of MSDSD in an ITU PedB channel

observed that with MSDSD it is possible to reach the point, where differential modulation offers a higher throughput than coherent detection, at a lower SNR. With CND the required SNR is about 34.5 dB, while with MSDSD the required SNR is about 33.3 dB. However, this SNR is still unrealistic for practical wireless systems.

## 4 Fast Fading

This chapter discusses the performance of differential modulation in fast fading channels. To this extent, Section 4.1 presents the proper selection of the modulation scheme for time varying channels. Section 4.2 considers the application of MSDSD in fast fading scenarios.

In fast fading, the coherence time  $T_c$  of the channel is assumed to be small enough, so that the impulse response of the channel changes significantly during a subframe. Thus, for the simulations in general an LTV channel is assumed. In this chapter, noncoherent detection is considered in an ITU VehA channel with different Doppler spreads  $D_s$  (see Chapter 3). We investigate the BER and the coded throughput over SNR.

### 4.1 Selection of the Differential Modulation scheme

In frequency selective LTV channels, the channel varies both in the frequency and in the time direction. The variation of the channel in the frequency direction depends on the delay spread  $T_d$  (see Section 3.1), while the variation in the time direction depends on the relative velocity  $v$  between transmitter and receiver. The velocity corresponds to the Doppler spread  $D_s$ .

As already described in Equation (2.21), varying channels introduce errors with noncoherent detection, irrespective of the noise. Furthermore, it was shown in Section 3.1 that the BER also depends on whether frequency first modulation or time first modulation is applied. Thus it is interesting to consider, which

modulation schemes is better suited for a fast fading environment.

#### 4.1.1 Frequency first versus time first modulation scheme in an ITU VehA channel

In fast fading scenarios, the choice of the modulation scheme depends on the delay spread  $T_d$  and on the Doppler spread  $D_s$  of the channel. As an illustration consider the coded throughput of both modulation schemes for a speed of 50 km/h and 150 km/h in an ITU VehA channel, depicted in Figure 4.1.

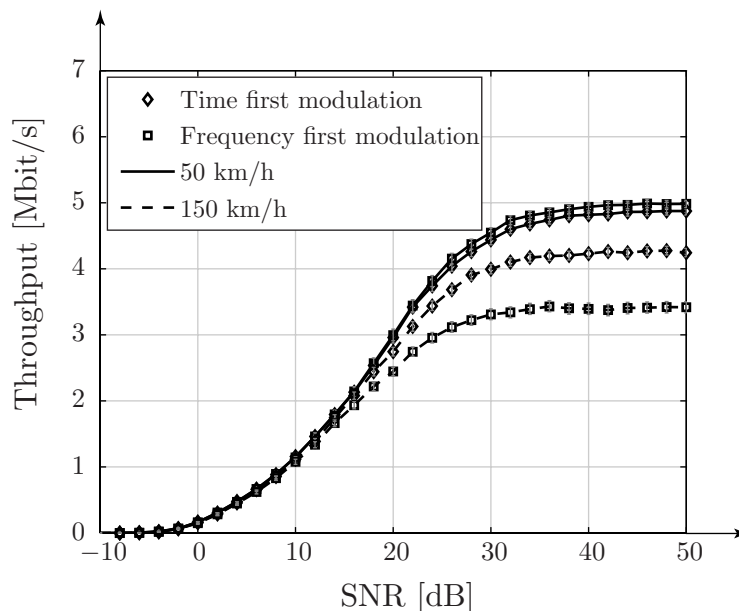


Figure 4.1: Coded throughput of the time first modulation versus the frequency first modulation in an ITU VehA channel

The simulation results show that at a speed of 50 km/h the throughput of the frequency first modulation is higher than the throughput of the time first modulation scheme. If the velocity is increased to 150 km/h, the time first modulation scheme outperforms the frequency first modulation scheme. This behavior can be explained by the correlation of the channel.

For low speeds, the correlation in the time direction is higher than it is in the frequency direction. This means, that the variation of the channel in the frequency direction is larger than in the time direction. In this case, modulation in the frequency direction is more likely to introduce errors than modulation in the time direction. Hence, it is better to use the frequency first modulation scheme, since here the modulation in the frequency direction occurs only once

(see Section 2.3). With increasing velocity the Doppler spread of the channel grows, which results in a lower correlation in the time direction. Thus, it is beneficial to change to the time first modulation scheme, since the larger variations of the channel in the time direction are effective only once, while modulating in the time direction.

As a conclusion, it is recommendable to use the modulation scheme that modulates most of the data in the direction with the highest correlation. For high frequency selective slowly fading channels, therefore, it is recommendable to use the frequency first modulation scheme, while for low frequency selective fast fading channels it is better to use the time first modulation scheme.

#### 4.1.2 Modulation scheme for AWGN channels, Rayleigh flat fading channels and channels with equal correlation

With the considerations of the previous section it can be concluded that for AWGN channels or block fading frequency flat Rayleigh channels the performance of differential modulation is the same, independent of the differential modulation scheme. This is because the channel neither changes in the time direction nor in the frequency direction. The same holds, if the correlation of the channel in the time direction and the frequency direction is equal. In this case, the probability of errors caused by the variation of the channel is the same in time and frequency direction.

#### 4.1.3 Estimation of the speed at which to switch between the frequency first and the time first modulation scheme

To estimate the speed at which it is recommendable to switch between the frequency first and the time first modulation scheme, we find the point where the correlation in time direction is equal to the correlation in frequency direction. From the autocorrelation matrix  $\Sigma_{\mathbf{hh}}^{(f)}$  in Equation (3.25) the correlation between two consecutive subcarriers in frequency direction can be calculated as

$$r_{hh}^{(f)}(1) = r_{hh}^{(f)*}(-1) = \mathbf{w}_2 \mathbf{H}_{PDP} \mathbf{w}_1^H. \quad (4.1)$$

In the equation above the superscript  $f$  indicates that the correlation is considered in frequency direction and  $\mathbf{w}_1$  and  $\mathbf{w}_2$  denote the first and second row

of the size  $K \times K$  DFT matrix, respectively. To calculate the autocorrelation in the time direction, the channel at each subcarrier  $k$  is considered as a frequency flat Rayleigh channel. This is justified because the LTE downlink is based on OFDM. OFDM systems convert a broadband frequency selective wireless channel into  $K$  orthogonal narrowband frequency flat channels by means of a FFT and application of a CP. The autocorrelation in the time direction can be calculated according to the Clarke's model [17] as

$$r_{hh}^{(t)}(\Delta n) = E\{H_{n,k}H_{n+\Delta n,k}^*\} = J_0(2\pi f_D T_S \Delta n). \quad (4.2)$$

Here,  $J_0(\cdot)$  is the Bessel function of zeroth order,  $f_D$  is the Doppler shift that can be calculated according to Equation (3.3) and  $T_S$  is the OFDM symbol duration. The variable  $\Delta n$  denotes the discrete time difference between two OFDM symbols and the superscript  $t$  indicates that the autocorrelation is considered in the time direction. Thus the correlation in time between two consecutive OFDM symbols is

$$r_{hh}^{(t)}(1) = r_{hh}^{(t)}(-1) = J_0(2\pi f_D T_S). \quad (4.3)$$

The velocity  $v$  where it is recommendable to change from one to the other modulation scheme is the solution to the equation

$$\begin{aligned} |r_{hh}^{(t)}(1)| &= |r_{hh}^{(f)}(1)| \\ |J_0(2\pi f_D T_S)| &= |\mathbf{w}_2 \mathbf{H}_{\text{PDP}} \mathbf{w}_1^H|. \end{aligned} \quad (4.4)$$

With Equation (3.3)  $v$  thus can be calculated as

$$v = \frac{c_0}{2\pi T_S f_c} J_0^{-1}(|\mathbf{w}_2 \mathbf{H}_{\text{PDP}} \mathbf{w}_1^H|) \quad (4.5)$$

As it can be seen  $v$  depends on the delay spread of the channel, which is represented by the PDP, the OFDM symbol duration  $T_S$  and the carrier frequency  $f_c$  of the system. A large delay spread of the channel, i.e., high frequency selectivity, means low correlation in the frequency direction. In this case it is recommendable to switch to the time first modulation scheme at higher velocities. On the other hand, if  $T_S$  grows, the correlation in the time direction gets smaller. This means that the channel variation in the time direction is

larger. Thus, for an increasing OFDM symbol duration it is better to use the time first modulation schemes already at lower speeds. The same effect occurs if the carrier frequency  $f_c$  of the system is increased. With increasing carrier frequency the Doppler shift increases as well. This leads to a higher Doppler spread which reduces the correlation in the time direction. Thus for a higher  $f_c$  it is also recommendable to switch to the time direction modulation at lower speeds. For an ITU VehA channel the result is  $v \approx 48\text{km/h}$ . In order to validate the results the BER for both modulation schemes was simulated at a SNR of 30 dB with different speeds. The results are presented in Figure 4.2. The simulation suggests a speed of about 51 km/h. The difference of the simulation results to the theoretical result can be explained by the accuracy of the simulations and additional correlations that are not considered due to the simple system model.

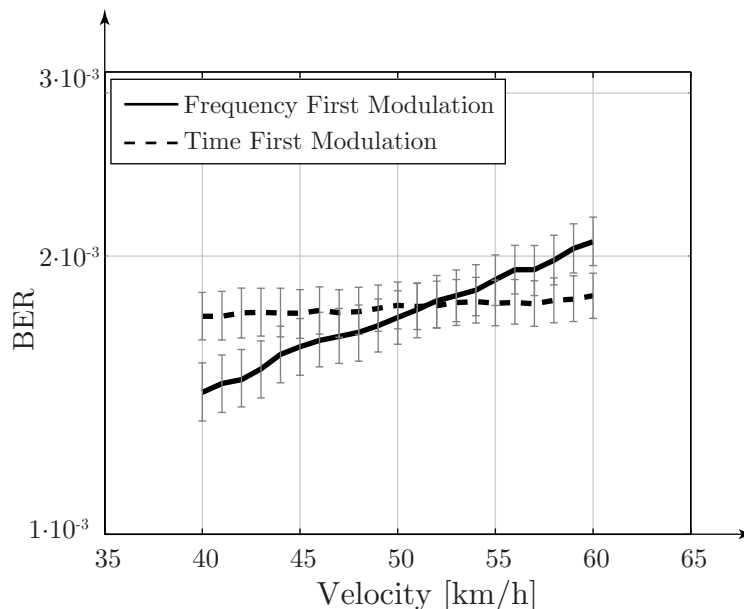


Figure 4.2: BER of frequency first versus time first modulation scheme in a fast fading ITU VehA channel with SNR = 30 dB

## 4.2 Multiple Symbol Differential Sphere Decoding in Fast Fading Channels

In order to improve the performance of noncoherent detection in this section MSDSD is considered. It is investigated, if MSDSD can achieve an performance gain compared to CND.

In fast fading channels, MSDSD is performed similarly as in block fading channels. The idea is to minimize the metric found in Equation (3.39) for DPSK and Equation (3.46) for DAPSK, respectively. For the detection in the frequency direction the autocorrelation matrix of the channel  $\Sigma_{\mathbf{hh}}^{(f)}$  can be calculated by Equation (3.25). For the detection in the time direction the autocorrelation matrix  $\Sigma_{\mathbf{hh}}^{(t)}$  can be calculated with the relation of Equation (4.3) as

$$\Sigma_{\mathbf{hh}}^{(t)} = \begin{pmatrix} r_{hh}^{(t)}(0) & r_{hh}^{(t)}(1) & \cdots & r_{hh}^{(t)}(N-1) \\ r_{hh}^{(t)}(-1) & r_{hh}^{(t)}(0) & \cdots & r_{hh}^{(t)}(N-2) \\ \vdots & \ddots & \ddots & \vdots \\ r_{hh}^{(t)}(-N+1) & r_{hh}^{(t)}(-N+2) & \cdots & r_{hh}^{(t)}(0) \end{pmatrix}, \quad (4.6)$$

Like in the block fading scenario, an observation window of  $N$  data symbols is used to detect  $N-1$  information symbols.

#### 4.2.1 Uncoded BER of 4-DPSK in an ITU VehA channel

The simulation results in Figure 4.3 show the uncoded BER of 4-DPSK in an ITU VehA channel with a speed of 100 km/h. According to the previous section, at this speed it is recommendable to use the time first modulation scheme. To validate this result, both the frequency first modulation and the time first modulation scheme are simulated and compared to coherent detection. For the noncoherent detection, CND as well as MSDSD with an observation window of  $N=4$  and  $N=8$  are applied.

The simulation results show that the BER of the time first modulation scheme is lower than that of the frequency first modulation scheme. This confirms that it is better to use the time first modulation scheme for this scenario. Furthermore, coherent detection outperforms noncoherent detection by about 2 dB. A comparison of MSDSD with CND for the time first modulation scheme at a BER of  $10^{-2}$  shows that the performance gain of MSDSD with  $N=4$  is about 0.1 dB. For an observation window of  $N=8$  the gain is about 0.3 dB. Similar to frequency selective channels, time selective channels lead to an error floor. The simulations show that for CND the error floor of the time first modulation scheme is lower than that of the frequency first modulation scheme. This is expected because of the previous simulation results. It is, however,



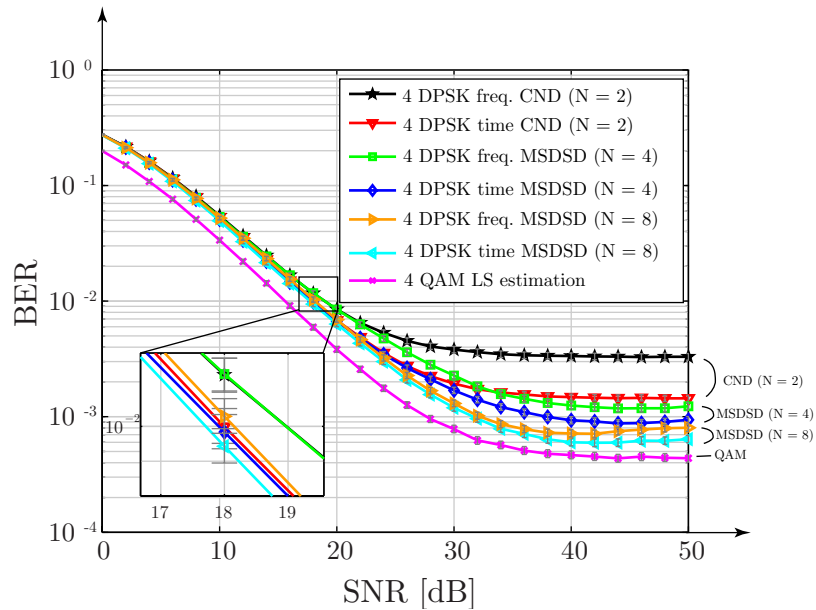


Figure 4.3: Uncoded BER performance of noncoherent detection in an ITU VehA channel with  $v = 100$  km/h

interesting to note that with MSDSD the difference of these error floors is smaller than with CND. This suggests that with MSDSD the exact selection of the modulation scheme dependent on correlation statistics of the channel is not as critical as with CND. The simulation results in [25, Figures 6-9] also confirm that result.

A last point to note is that the error floor of fast fading channels cannot be mitigated by MSDSD, even with large observation window sizes. Simulations in [25] show, that although MSDSD is able to alleviate the performance loss due to the reduced correlation in the time direction, it is not able to reduce the effect of ICI. In [25] it was also shown that with incorporation of the ICI into the correlation matrix it is possible to further increase the performance and to decrease the error floor, however, at the cost of complexity of the detection process. Simulations to that regard were not considered in this thesis.

#### 4.2.2 Coded throughput in an ITU VehA channel

Figure 4.4 shows the coded throughput of MSDSD in an ITU VehA channel with a speed of 100 km/h. The observation window size for 4-DPSK is set to both  $N = 4$  and  $N = 8$  and to  $N = 4$  for 16-DAPSK. Due to the long simulation time, MSDSD for 64-DAPSK was not simulated. The simulations are compared to coherent detection. As modulation scheme the time first

modulation scheme is applied

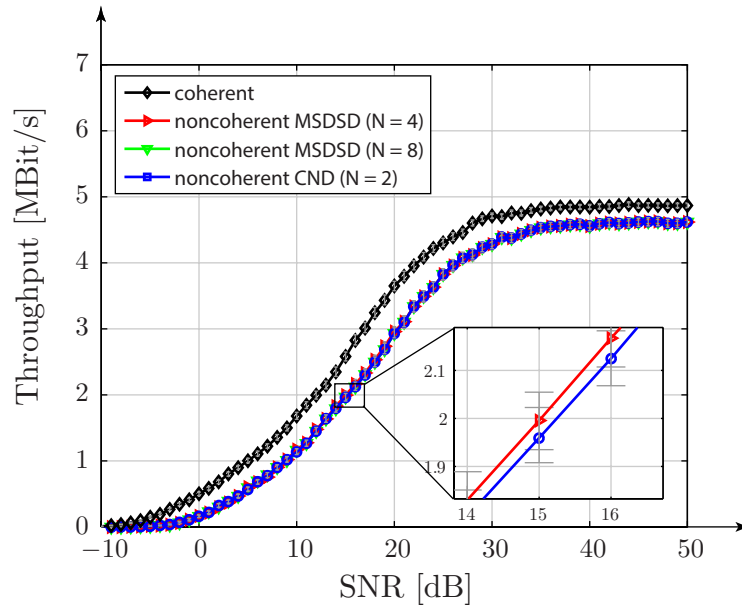


Figure 4.4: Coded throughput of MSDSD in an ITU VehA channel for  $v = 100$  km/h

The simulation results show that for fast fading scenarios noncoherent detection performs worse than coherent detection. The performance loss of noncoherent detection to coherent detection is about 3.5 dB at a throughput of 3 Mbit/s. Because of the high time selectivity of the channel, the originally offered higher throughput of differential modulation cannot be achieved. In fact, noncoherent detection loses about 4.5 % compared to coherent detection in peak throughput. The performance gain of MSDSD compared to CND at a throughput of 0.8 Mbit/s is about 0.1 dB for  $N = 4$  and about 0.2 dB for  $N = 8$ . At a throughput of 2 Mbit/s (here 16-DAPSK determines the throughput), the gain of MSDSD with  $N = 4$  is 0.2 dB.

With the simulation results it can be concluded, that in fast fading scenarios MSDSD does not provide a significant performance gain compared to CND.

## 5 Conclusion

In this diploma thesis, we evaluated the performance of differential modulation applied to an OFDM system that is similar to the LTE downlink. In our discussions, we first presented a general description of differential modulation and showed how it can be applied to the LTE downlink in SISO systems. We presented two basic differential modulation schemes, namely the time first and the frequency first modulation scheme and discussed their applicability to LTI channels.

In our investigations, we found that for frequency selective LTI channels it is better to use the frequency first modulation scheme, since in this case the variation of the channel is less effective. For frequency flat channels like AWGN and Rayleigh flat channels the performance of differential modulation does not depend on the modulation scheme. We showed that coherent detection in general outperforms CND, where 2 received data symbols are used to detect one information symbol. In order to improve the performance of noncoherent detection, we applied MSDD, where  $N$  data symbols are used to jointly detect  $N - 1$  information symbols. The disadvantage of MSDD is the exponential complexity growth with the number of observed symbols  $N$ . To circumvent that problem, we used MSDSD, which significantly reduces the complexity of the phase detection process by the application of the SD algorithm. With the simulation results we showed that the performance of differential modulation can be improved especially for AWGN channels. However, although MSDSD was used, coherent detection still performs better than noncoherent detection in terms of coded throughput.

In the last chapter, we discussed the performance of differential modulation in fast fading scenarios. We showed that in frequency selective LTV channels the selection of the modulation scheme depends both on the delay spread and the Doppler spread of the channel, and the applied detection scheme. We found that it is preferable to use the differential modulation scheme, which modulates most of the data in the direction with the highest correlation. That means, e.g., for frequency selective slowly fading channels it is better to use the frequency first modulation scheme. On the other hand, the time first modulation scheme is better suited for LTV channels, where the variation of the channel in the time direction is less than in the frequency direction. We also gave an calculation at which speed it is beneficial to switch from one modulation scheme to the other. With the simulations we realized that the correct selection of the modulation scheme is more critical for CND than for MSDD, i.e., MSDD is more robust to a wrong selection of the modulation scheme. The simulation results showed that also in fast fading scenarios, coherent detection outperforms noncoherent detection. The performance gain of MSDSD compared to CND is lower, since the channel correlation is smaller.

Thus in conclusion, although differential modulation provides a gain in spectral efficiency, with the techniques presented in this thesis, differential modulation is not a competitive alternative to coherent detection in the LTE downlink.

In possible further work, the performance of differential modulation could be investigated with a channel correlation matrix that incorporates the inter carrier interference. Additionally, the symbol alphabet could be adapted according to the channel statistics. That means, if the channel correlation in one direction is high, a larger symbol alphabet could be applied in this direction. Lastly, differential modulation could be investigated for the MIMO LTE downlink.

# Appendix A

## Acronyms

**ASK** Amplitude Shift Keying

**APSK** Amplitude and Phase Shift Keying

**BER** bit error ratio

**BDPSK** binary Differential PSK

**BLER** block error rate

**CND** conventional noncoherent detection

**CP** cyclic prefix

**CQI** channel quality indicator

**DAPSK** Differential Amplitude and Phase Shift Keying

**DASK** Differential Amplitude Shift Keying

**DFT** Discrete Fourier Transform

**DPSK** Differential Phase Shift Keying

**FIR** finite impulse response

**FFT** Fast Fourier Transform

**ICI** inter carrier interference

**IFFT** Inverse Fast Fourier Transform

**ISI** inter symbol interference

**LS** least squares

**LTE** Long Term Evolution  
**LTI** linear time-invariant  
**LTV** linear time-variant  
**M-APSK** *M*-Amplitude and Phase Shift Keying  
**M-DAPSK** *M*-Differential Amplitude and Phase Shift Keying  
**M-PSK** *M*-Phase Shift Keying  
**ML** maximum likelihood  
**M-QAM** *M*-Quadrature Amplitude Modulation  
**MLSE** maximum likelihood sequence estimator  
**MIMO** multiple input multiple output  
**MSDD** multiple symbol differential detection  
**MSDSD** multiple symbol differential sphere decoding  
**OFDM** Orthogonal Frequency Division Multiplexing  
**PDP** power delay profile  
**PSK** Phase Shift Keying  
**QAM** Quadrature Amplitude Modulation  
**RB** resource block  
**RBP** resource block-pair  
**RE** resource element  
**RS** reference symbols  
**RFF** Rayleigh flat fading  
**SISO** single input single output  
**SD** sphere decoding  
**SNR** signal-to-noise ratio  
**UMTS** Universal Mobile Telecommunications System  
**WSSUS** wide-sense stationary uncorrelated scattering  
**ZF** zero forcing

# Bibliography

- [1] CISCO, “**Global mobile data traffic forecast update 2011 - 2016**,” Tech. Rep., Feb. 2012.
- [2] IDATE and UMTS Forum, “**Mobile traffic forecasts 2010 - 2020**,” Tech. Rep., 2011.
- [3] 3GPP, “**Technical Specification Group Radio Access Network; (E-UTRA) and (E-UTRAN); Overall Description; stage 2**,” Tech. Rep., Sep. 2008.  
<http://www.3gpp.org/ftp/Specs/html-info/36300.htm>
- [4] T. May, H. Rohling, and V. Engels, “**Performance analysis of Viterbi decoding for 64-DAPSK and 64-QAM modulated OFDM signals**,” *IEEE Transactions on Communications*, vol. 46, no. 2, pp. 182–190, Feb. 1998, doi: 10.1109/26.659477.
- [5] M. Lott, “**Comparison of frequency and time domain differential modulation in an OFDM system for wireless ATM**,” in *1999 IEEE 49th Vehicular Technology Conference*, vol. 2, pp. 877–883 vol.2, Jul. 1999, doi: 10.1109/VETECC.1999.780469.
- [6] J. Proakis, **Digital Communications**, 4th ed. McGraw-Hill Science/Engineering/Math, Aug. 2000. ISBN: 0072321113.
- [7] H. Rohling and V. Engels, “**Differential amplitude phase shift keying (DAPSK)-a new modulation method for DTVB**,” in *1995. IBC 95. International Broadcasting Convention*, pp. 102–108. IET, 1995. doi: 10.1049/cp:19950937.
- [8] R. Fischer, L.-J. Lampe, and S. Muller-Weinfurtner, “**Coded modulation for non-coherent reception with application to OFDM**,” *IEEE Transactions on Vehicular Technology*, vol. 50, no. 4, pp. 910–919, Jul. 2001, doi: 10.1109/25.938568.
- [9] L. Wang and L. Hanzo, “**Low-Complexity Near-Optimum Multiple-Symbol Differential Detection of DAPSK Based on Iterative Amplitude/Phase Processing**,” *IEEE Transactions on Vehicular Technology*, vol. 61, no. 2, pp. 894–900, Feb. 2012, doi: 10.1109/TVT.2011.2181192.
- [10] E. Dahlman, S. Parkvall, and J. Sköld, **4G LTE/LTE-Advanced for Mobile Broadband**, ser. Academic Press, ISBN: 9780123854896.
- [11] A. Molisch, **Wireless Communications, Second Edition**. John Wiley & Sons Ltd., 2011. ISBN: 9780470741870.
- [12] C. Schlegel and L. Perez, **Trellis and Turbo Coding**, ser. IEEE Series on Digital & Mobile Communication. Wiley, 2004. ISBN: 9780471667834.  
<http://books.google.at/books?id=Lz6ax96ITBUC>
- [13] ITU, “**Recommendation ITU-R M.1225: Guidelines for Evaluation of Radio Transmission Technologies for IMT- 2000 Systems**,” International Telecommunication Union, Recommendation ITU-R M.1225, 1998.

- [14] Y. Ma, Q. Zhang, R. Schober, and S. Pasupathy, “**Performance analysis of DAPSK over general fading channels,**” in *IEEE International Conference on Communications*, vol. 5, pp. 3580 – 3584 vol.5, May 2003, doi: 10.1109/ICC.2003.1204120.
- [15] 3GPP, “**Evolved Universal Terrestrial Radio Access (E-UTRA); Physical layer procedures,**” 3rd Generation Partnership Project (3GPP), TS 36.213 Version 10.2.0, Jun. 2011.  
<http://www.3gpp.org/ftp/Specs/html-info/36213.htm>
- [16] M. Simko, “**Channel estimation for UMTS Long Term Evolution,**” Master’s thesis, Institut für Nachrichtentechnik und Hochfrequenztechnik, Vienna University of Technology, 2009.
- [17] D. Tse and P. Viswanath, **Fundamentals of Wireless Communication.** Cambridge University Press, Jun. 2005. ISBN: 0521845270.
- [18] D. Divsalar and M. Simon, “**Multiple-symbol differential detection of MPSK,**” *IEEE Transactions on Communications*, vol. 38, no. 3, pp. 300–308, Mar. 1990, doi: 10.1109/26.48887.
- [19] P. Ho and D. Fung, “**Error performance of multiple-symbol differential detection of PSK signals transmitted over correlated Rayleigh fading channels,**” *IEEE Transactions on Communications*, vol. 40, no. 10, pp. 1566 –1569, Oct. 1992, doi: 10.1109/26.168784.
- [20] Y. Li, J. Cimini, L.J., and N. Sollenberger, “**Robust channel estimation for OFDM systems with rapid dispersive fading channels,**” *IEEE Transactions on Communications*, vol. 46, no. 7, pp. 902 –915, Jul. 1998, doi: 10.1109/26.701317.
- [21] L. Lampe, R. Schober, V. Pauli, and C. Windpassinger, “**Multiple-symbol differential sphere decoding,**” in *IEEE International Conference on Communications*, vol. 2, pp. 787 – 791 Vol.2, Jun. 2004, doi: 10.1109/ICC.2004.1312609.
- [22] B. Hochwald and S. ten Brink, “**Achieving near-capacity on a multiple-antenna channel,**” *IEEE Transactions on Communications*, vol. 51, no. 3, pp. 389 – 399, Mar. 2003, doi: 10.1109/TCOMM.2003.809789.
- [23] C. P. Schnorr and M. Euchner, “**Lattice basis reduction: Improved practical algorithms and solving subset sum problems.**” in *Math. Programming*, pp. 181–191, 1993.
- [24] V. Pauli, L. Lampe, and R. Schober, “**“Turbo DPSK“ using soft multiple-symbol differential sphere decoding,**” *IEEE Transactions on Information Theory*, vol. 52, no. 4, pp. 1385 – 1398, Apr 2006, doi: 10.1109/TIT.2006.871048.
- [25] A. Ishii, H. Ochiai, and T. Fujino, “**Performance analysis of multiplesymbol differential detection for OFDM over both time- and frequencyselective Rayleigh fading channels,**” *EURASIP Journal on Applied Signal Processing*, vol. 2004, pp. 1536–1545, Sep. 2004.